Identification of Subcellular Compartments Containing Disseminated α-Synuclein Seeds by Proteomic Analysis

DOCTORAL DISSERTATION

A thesis submitted in partial fulfillment
of the requirements for the degree of
Doctor of Philosophy

By:
Junya Kasahara

Supervisor:
Dr. Nobuyuki Nukina

Co-Supervisor:
Dr. Yukio Imamura,
Dr. Tomoyuki Yamanaka,
and
Dr. Haruko Miyazaki

Graduate School of Brain Science
Doshisha University
March 2021
Kyoto, Japan

Table of Contents

List of Figures and Tables

Abbreviations

PD; Parkinson disease

DLB; Dementia with Lewy bodies

a-syn; Alpha-synuclein

WT; wild type

NAC; hydrophobic non-amyloid component

PFFs; pre-formed fibrils

QD-a-syn PFFs; Quantum dots-labeled a-syn pre-formed fibrils

GO; Gene ontology

FAOS; fluorescence-activated organelle sorting

ips; ipsilateral side

co; contralateral side

Abstract

The pathological form of a-synuclein (a-syn) is transmitted through neural circuits in the brains of Parkinson disease (PD) patients and amplifies misfolded a-syn, further forming intracellular deposits. The transmission mechanism of a-syn pre-formed fibrils (PFFs) has been investigated by cellular and animal models of PD. However, the details of a-syn PFFs transmission *in vivo* have not been fully elucidated since a-syn PFFs, seeds of the a-syn pathology, are difficult to detect in a reliable manner.

In this thesis, in order to clarify how a-syn PFFs are transmitted and propagated throughout the mammalian brain, I analyzed the subcellular distribution of a-syn PFFs in the brain by using Quantum dots (QD) labeled a-syn PFFs (QD-a-syn PFFs) as an optical tracer. Six hours after inoculating QD-a-syn PFFs into the unilateral striatum of wild-type mouse brain, I could detect particles positive for QD-a-syn PFFs in brain homogenates obtained from the ipsilateral and contralateral sides of the brain. I then purified QD-a-syn PFFs-enriched particles from both hemispheres with fluorescence-activated organelle sorting. Proteomic analysis of these particles suggested that the QD-a-syn PFFs-positive particles derived from the contralateral sides contained components of the synapse, whereas the QD-a-syn PFFs-positive particles obtained from the ipsilateral sides contained proteins residing in the endoplasmic reticulum (ER). The validation of

identified proteins by proteomic analysis by immunostaining of the brain sections further confirmed that the QD-a-syn PFFs in the contralateral side colocalized with synaptic vesicle marker proteins in the cortex and striatum. Contrarily, the QD-a-syn PFFs in the ipsilateral side preferentially colocalized with ER marker proteins. These results were largely consistent with those from the proteomic analysis.

In summary, this study revealed potential molecular candidates responsible for the dissemination of a-syn PFFs at the initial phase of a-syn transmission during the PD pathology. Further detailed studies of candidate proteins in the context of a-syn transmission will provide potential molecular therapies to prevent the progression of PD.

Acknowledgements

I would like to show my greatest appreciation to my advisors, Professor Nobuyuki Nukina, Dr. Yukio Imamura, Associate Professor Tomoyuki Yamanaka, and Assistant Professor Haruko Miyazaki for providing the experimental knowledge and advices when planning my experiments. Sometimes they were strict but I believe that they encouraged me throughout my experiments and improved my skills as a Ph.D. I wish to express my heartfelt gratitude to professors in Graduated School of Brain Science, Doshisha University. I truly appreciate their comments, opinions and feedback of my experiments that improved the quality of my thesis.

I would also like to thank Akiko Hiyama for technical assistance of my experiments, RIKEN BMA Mass Spectrometry Service especially Kaori Otsuki for LC-MS/MS analysis.

This work was supported by Japan Agency for Medical Research and Development, AMED under Grant Number JP20dm0107140 to N.N. and from the Ministry of Education, Culture, Sports, Science and Technology (MEXT) of Japan to N.N.(17H01564) to T.Y. (15K06702, 17KT0131). Fluorescence-activated cell sorting (SH800S) was performed at the Medical Research Support Center, Graduate School of Medicine, Kyoto University, which was supported by Platform for Drug Discovery,

Informatics, and Structural Life Science from the Ministry of Education, Culture, Sports, Science and Technology, Japan.

Finally, I would like to express my gratitude to my friends and family for their comments, support and encouragement throughout my work. Especially, I thank Dr. Hongsun Park and Edward William Ko Uy for English editing of the manuscript.

Chapter 1. Introductions

1.1. Parkinson disease and a-synuclein pathology

Parkinson disease (PD) is one of the most common neurodegenerative diseases with movement disturbances including rigidity, resting tremor and gait disturbance. PD was first described by James Parkinson in 1817, and it is estimated that the disease affects approximately 6 million people worldwide. The incidence of PD is rarely seen in patients under the age of 40 but increases with age (Hayes, 2019). In fact, the disease affects 1 % of the population of people over 60 years old (Tysnes and Storstein, 2017). Therefore, there is a risk that PD affects people of certain age in many countries, especially those in aging society, resulting in a substantial increase of patients around the world. Although many researchers have been trying to develop treatment of PD, there are still no effective medicines or cures, and only symptomatic treatment that prevents progression of neuronal degeneration is available.

Despite the lack of efficient medicines, accumulated studies gradually certify the progression of PD pathology. One of the main pathological features of PD is progressive neuronal degeneration in substantia nigra (Goedert, 2015, Braak and Del Tredici, 2017) with Lewy bodies and Lewy neurites, which are deposits of misfolded alpha-synuclein (a-syn) (Spillantini et al., 1997). The a-syn pathology spread from olfactory nucleus and vagal nerve in the early stages of the disease, and further spreads

to nuclear grays and cortical areas in the late stages (Braak et al., 2003). Also, a substantial fraction of PD patients develops dementia, which is explained by the fact that the a-syn pathology in the cortical areas correlates with the development of dementia (Irwin et al., 2012). Furthermore, the existence of familial cases with a-syn missense mutations or increased gene dosage such as duplication or triplication of a-syn gene suggests that a-syn depositions should have a significant role in the pathological process of PD (Singleton et al., 2003, Muñoz et al., 1997, Polymeropoulos et al., 1997). Taken together, although it is still unclear how the a-syn deposits result in various disease phenotypes, the localization and abundance of a-syn deposits are prone to correlate with clinical symptoms and progression of PD. Thus, many studies have focused on the a-syn pathology to understand the relationship between the pathological protein and PD.

1.2. A-syn protein

A-syn is composed of 140 amino acids and encoded by the human alpha-synuclein gene (*SNCA*). Generally, a-syn localizes in the central nervous system, mainly in presynaptic nerve terminals. This protein has several functions such as modulation of calmodulin activity, synaptic maintenance, mitochondrial homeostasis, modulating vesicle trafficking and chaperone activity (Emamzadeh, 2016).

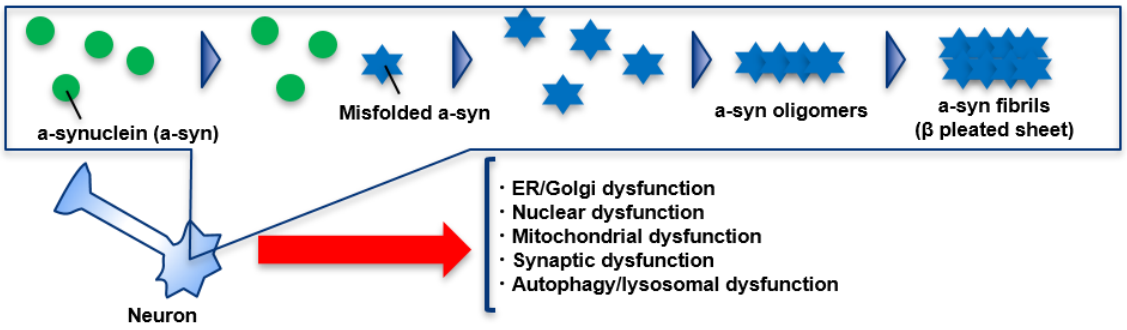

Figure. 1 Formation of a-syn fibrils that cause several cellular dysfunctions.
The summary of a-syn fibril formation and a-syn cellular toxicity are shown. Modified a-syn deposits in cells are implicated to several pathologies. The scheme was modified from the previously reported work (Wong and Krainc, 2017).

A-syn is composed of three major regions: an amphipathic alpha-helix region, a hydrophobic non-amyloid component (NAC) domain and an acidic region, and this protein is natively unfolded (Burré et al., 2014). Under disease conditions, a-syn proteins are converted into misfolded a-syn from its native state, and the misfolded a-syn proteins become capable of interacting each other to form oligomers, further forming beta-sheet-rich fibrils (Figure.1). These oligomers and fibrils are so-called amyloid, fibrous protein that is insoluble in water and exhibit cross-beta sheet structures. Although the exact structure of the misfolded a-syn has not been determined at atomic levels, it is likely that slight conformational changes of amyloid would result in the formation of a misfolded intermediate (Soto, 2001). These a-syn oligomers and fibrils are considered as pathological a-syn, and the biochemical and structural characteristics of these endogenous pathologically deposited proteins are also still unclear.

The exact molecular structures of a-syn aggregates that cause neurotoxicity in the process of aggregation remains ambiguous. However, recombinant a-syn pre-formed fibrils (a-syn PFFs) have been also used as pathological a-syn. Neuronal models incubated with a-syn PFFs undergo cellular dysfunction (Wong and Krainc, 2017), and also the injection of PFFs into the mouse brain causes behavioral abnormalities and accumulation of a-syn aggregates in animal models (Luk et al., 2012). By using the same methods, mice inoculated with a-syn PFFs by insertion of a single needle into the right striatum showed phosphorylated a-syn (P-syn) deposits, an indicator of a-syn aggregation, six months after the injection. Interestingly, the a-syn deposits were found not only in the striatum, but also in the different brain regions including cortex, substantia nigra, entorhinal cortex and amygdala. (Okuzumi et al., 2018, Henderson et al., 2019). These studies indicate that the a-syn PFFs cause cellular dysfunction and spread through the neuronal connections, further inducing a-syn pathology *in vivo*. Therefore, many studies have used the a-syn PFFs as pathological seeds of a-syn to reveal the dynamics of a-syn seeds.

1.3. The transmission of a-syn

Clinical reports showed that fourteen years after transplantation of solid pieces of human ventral mesencephalon into the striatum of an individual with PD, grafted nigral

neurons were found to have Lewy body–like inclusions, suggesting that the pathological a-syn seeds, the cause of Lewy body formation, were transmitted from the neighboring host neurons to the grafted neurons (Kordower et al., 2008, Li et al., 2008). In primary neurons, a-syn PFFs can be internalized into cell bodies and nerve terminals, and further time-dependently induce formation of endogenous a-syn fibrils in cell bodies or axons (Volpicelli-Daley et al., 2011). In addition, a-syn PFFs are transported in both anterograde and retrograde directions in primary neurons (Brahic et al., 2016). These features are also observed in neurons derived from human induced pluripotent stem cells (Gribaudo et al., 2019).

In addition to various transmission mechanisms described above, accumulated evidence has indicated that pathological a-syn can be transmitted through various cellular mechanisms. For instance, exosomes derived from the patients of Dementia with Lewy Bodies (DLB) contained a-syn, and injection of these exosomes into mouse brains caused the accumulation of P-syn (Ngolab et al., 2017), indicating the involvement of exosomes in the transmission of a-syn. Furthermore, an activation of microglial cells by lipopolysaccharide and the subsequent ablation of these microglia affected the cell-to-cell transfer of human a-syn in the mouse brain (George et al., 2019), indicating that, in addition to the direct inter-neuronal transmission, microglia is also involved in the

transmission of a-syn. As such, various cell types as well as cellular mechanisms have been proposed to be responsible for the transmission of a-syn seeds.

1.4. Aims of this thesis

Although it is widely accepted that a-syn seeds spread within the nervous system, the precise mechanism of a-syn seeds transmission in the brain is still unclear. In a previous study from the Nukina laboratory, Okuzumi et al. injected a-syn PFFs as seeds into the unilateral striatum of the mouse brain and found that a-syn seeds were transmitted from the ipsilateral hemisphere of the injection to the contralateral side through the corpus callosum within a day (Okuzumi et al., 2018), indicating that a-syn seeds were transported along the neuronal axons from the ipsilateral to the contralateral side of the brain. Although the seeds eventually induced the accumulation of pathological P-syn in both hemispheres, the initial distribution of the seeds before the onset of pathological P-syn accumulation was not investigated.

In this thesis, I aimed at clarifying the molecular and cellular mechanisms underlying transmission of a-syn PFFs observed in Okuzumi et al. study. To this end, I labeled a-syn PFFs with Quantum dots 705 (QD-a-syn PFFs) which is highly bright and less prone to photobleaching. Six hours, instead of one day, after the injection of QD-a-syn PFFs into the right striatum of mouse brains, I succeeded in isolating the particles

positive for QD-a-syn PFFs from both sides of the injected brain. I then performed comprehensive proteomic analysis on these particles to clarify the subcellular localization of QD-a-syn PFFs in both sides of the brain. I found that the proteins enriched in these particles included ER-related proteins in the ipsilateral side, whereas those enriched in the contralateral side were categorized into proteins associated with synapses or neuronal function-related proteins. The current findings suggest that a-syn PFFs transmission *in vivo* could be associated with the synaptic region and is disseminated through the neuronal system.

Chapter 2. Material and methods

2.1.Antibodies

The following antibodies were used: anti-Human-alpha synuclein antibody (18-0215, Invitrogen), anti-ERp57 (ab10287, Abcam), anti-Synapsin-1 (VAP-SV060E, Stressgen), anti-PSD-95 antibody (610495, BD Transduction Laboratories), anti-Tom20 (sc-11415, Santa Cruz Biotechnology), anti-CD81 (sc-7637, Santa Cruz Biotechnology), anti-Iba-1 antibody (019-19741, Wako) and anti-Synaptophysin-1 (101011, Synaptic Systems).

2.2. Purification of recombinant a-syn

The methods for purification of His-tagged human-a-syn and the formation of a-syn PFFs has been described previously (Okuzumi et al., 2018). E. coli BL21 (DE3) were transformed with the expression vector pET-15b, encoding human a-syn, cultured overnight in 25 ml LB medium including 50 μg/ml ampicillin (LB amp+) and transferred to 250 ml LB amp+. 1 mM Isopropyl-β-D-thiogalactopyranoside was added, and the mixture was incubated for 6 h at 37 °C and then centrifuged at 3,000 x g for 30 min at 4 °C. Cells were lysed with Phosphate-buffered saline (PBS) containing 2 % TritonX-100 and centrifugated at 20,000 x g for 30 min at 4 °C. The supernatant was further loaded on a Ni-sepharose 6 Fast Flow column (1 ml, GE Healthcare). A-syn was then eluted using

buffer A [50 mM Tris-HCl (pH 8.0), 100 mM NaCl] including 250 mM imidazole, further concentrated via centrifugation at 3,000 x g for 15 min with Vivaspin Turbo tubes (15 K MW) (50 ml, Sartorius). The collected a-syn was treated with thrombin agarose (Sigma) and rotated for 20 h at 20 °C to cleave the N-terminal His-tag.

2.3. Preparation for human-a-syn-PFFs and labeling of PFFs with QD

Purified a-syn monomers (100 µM, 150 µl) were agitated in buffer A with plastic beads (Sanplatec) using DWMax M•BR-034 (TAITEC) at 1,000 rpm for 7 days at 37 °C. Aggregates were pelleted by ultracentrifugation at 153,700 x g for 1 h at 4 °C, resuspended in buffer A (150 µl) and then ultracentrifuged at the same condition again. These aggregates were resuspended in buffer A (150 µl) and sonicated using Bioruptor (Biorad). They were used in experiments as 'pre-formed fibrils (PFFs)'. PFFs were coupled with Quantum dots (QD) (Cadmium selenium telluride, CdSeTe-COOH, Thermo Fisher Scientific), which emits maximum fluorescence intensity at 705 nm, using Amine Coupling Kit (DOJINDO). The precise characterization of QD-a-syn PFFs will be published elsewhere (Imamura et al. unpublished).

2.4. Animals

8-week-old male C57BL/6J mice were obtained from CLEA Japan, Inc. The mice were housed under a 12-h light/12-h dark cycle with access to food and water and at a maximum of five per cage. The breeding and housing of the mice were done according to the guidelines for Animal Care of Doshisha University, and the experiments were approved by the Doshisha University Animal Care and Use Committee. Only male mice were used for this study.

2.5. Inoculation of QD-a-syn PFFs into mouse brain

The method of a-syn PFFs injection into mouse brain has been described previously (Okuzumi et al., 2018). For intracerebral injection, QD-a-syn PFFs were sonicated using Bioruptor (Biorad) until an isocratic solution was obtained. Mice were anesthetized using three types of mixed anesthetic agents (0.3 mg/kg of medetomidine, 4.0 mg/kg of midazolam and 5.0 mg/kg of butorphanol) (Kawai et al., 2011) via peritoneal injection, and 2 μl of QD-a-syn PFFs (5 μg/μl) were injected unilaterally into the right striatum (A-P: 0.3 mm; M-L + 2 mm; D-V: − 2.5 mm, from bregma) using a 10 μl Hamilton syringe at a rate of 0.5 μl per min. Control mice received sterile PBS instead of QD-a-syn PFFs. After pre-determined time points (6 hours), the anesthetized mice were perfused with PBS.

Mouse brains were removed, and a part of brain (A-P: ± 4 mm from the seeds injection point) including cerebrum and the part of olfactory bulb and midbrain was obtained. The obtained brains were further separated into each hemisphere, in other words, ipsilateral and contralateral sides to the injected side.

2.6. Preparation of subcellular fractionation containing QD-a-syn PFFs

Based on the protocol reported previously (Gylys and Bilousova, 2017, Kahle et al., 2000), I filtrated homogenization buffer [9 % Sucrose, 25 mM Tris-HCl (pH 7.0), 5 mM dithiothreitol (DTT), 2 mM EDTA and protease inhibitors, cOmplete™ (1 tablet/50 ml, Sigma-Aldrich)] with 0.45 μm pore size filters (PVDF) (Millipore) to avoid non-specific signal while cell sorting. Mouse brain in nine volumes (v/w) of homogenization buffer were homogenized 10 cycles with Potter-Elvehjem tissue grinder on ice. The homogenates filtrated through 40 μm nylon mesh (Falcon) were designated as total fraction. Total fraction was centrifuged at 1,000 x g for 5 min at 4 °C and the pellets (P1) were collected. The supernatants (S1) were centrifuged at 12,500 x g for 15 min at 4 °C, and crude synaptosome enriched pellet (P2) and supernatant (S2) were obtained. The procedure of subcellular fractionation is summarized in Figure.4. For counting QD-a-syn

PFFs in P2 and S2 homogenates, 5 μg proteins were spotted on a glass slide, covered with a cover glass, and further observed with KEYENCE BZ-X710 fluorescence microscope.

2.7. Western blotting analysis

Brain homogenates were diluted in SDS-containing Laemmli buffer [final; 100 mM Tris-HCl (pH 6.8), 4 % SDS, 2 % 2-mercaptoethanol, 20 % glycerol and 0.01 % bromophenol blue] to make final samples (protein concentration; 0.75 mg/ml). Samples (10-15 μl) after boiling were loaded onto 12 % SDS containing polyacrylamide gels (6.25 % stacking gel) and separated at 40 mA for 60 min at room temperature with running buffer (100 mM Tris, 100 mM glycine and 0.1 % SDS). Proteins in the gels were transferred onto a PVDF membrane for 60 min at 25 V at room temperature. The membranes were blocked in 5 % skim milk in 0.05 % Tween 20/Tris-buffered saline (TBST) or 5 % Goat serum in 0.05 % TBST and incubated with primary antibodies (dilution 1:1,000) overnight at 4 °C. The membranes were washed three times in TBST and incubated for 1 h with horseradish peroxidase-conjugated secondary antibody (dilution 1:2,000). Immunoreactive proteins were visualized using a chemiluminescence reagent, Luminata (Millipore). Chemiluminescent signals were obtained using ImageQuant LAS-4000 (GE Healthcare).

2.8. Fluorescence-activated organelle sorting analysis

I performed fluorescence-activated organelle sorting (FAOS) (Satori et al., 2012) to enrich the fraction containing QD-a-syn PFFs (Gylys and Bilousova, 2017). Homogenates of P2 fraction were directly subjected to fluorescence-activated cell sorter SH800S (Sony) with a sorting chip of 100 μm diameter (LE-C3210, Sony). While the sorting process is in progress, the homogenates were kept at 4 °C, and 488 nm laser was used for detection of forward scatter (FSC) and back scatter (BSC). Threshold of particles was determined by fluorescence intensity from 690 to 750 nm based on the sorting results of negative/positive control. Homogenates of brain to which PBS or QD-a-syn PFFs in PBS were inoculated respectively. 10,000 events of sorting results were analyzed by Cell sorter software (Sony). QD-positive particles in ipsilateral or contralateral hemisphere were collected from 2 to 3 or from 5 to 8 mice brains, respectively. The sorting samples were ultracentrifuged (153,700 x g for 20 min). The collected pellets were diluted in homogenization buffer, and 5 μg proteins of samples were spotted on slide glass and observed with KEYENCE BZ-X710 fluorescence microscope to validate the concentration of QD-a-syn PFFs by sorting.

2.9. Mass spectral analysis of proteins

Protein digestion was referred to Filter-aided Sample Preparation (FASP) method (Wiśniewski et al., 2009). To concentrate sorted QD-a-syn PFFs particles, 1 ml of sorted solution was subjected to ultracentrifuge (153,700 x g for 20 min), and the pellets were collected. The pellets were diluted in SDS-lysis buffer [4 % SDS, 100 mM Tris-HCl (pH 7.6), and 0.1 M DTT), further heated at 95℃ for 5 min. Samples were mixed with 200 µl of 8 M urea in 100 mM Tris-HCl, pH 8.5 (UA) in the filter unit (molecular weight cut-off 30 kDa, PT-1007, Aproscience) and centrifuged at 14,000 x g for 15 min for two times. The flow-through from the collection tube was discarded, and 100 µl IAA solution (0.05 M Iodacetamide in UA) was added, vortexed mildly for 1 min, and incubated for 20 min in the dark. The filter unit was spun at 14,000 x g for 10 min with 100 µl of UA and centrifuged at 14,000 x g for 15 min twice. It was subjected to the addition of 50 mM ammonium bicarbonate (AmBic) in milli-Q water twice. Residual proteins were enzymatically digested by 40 µl of 100 ng/µl modified trypsin (V511A, Promega) in 50 mM acetic acid overnight at 37 ℃. To collect the resulting peptides, the filter unit was subjected to the addition of 50 mM AmBic and centrifuged at 14,000xg for 10 min twice. After adding 50 µl 0.5 M NaCl and centrifuging at 14,000 x g for 10 min, the flow through including digested proteins was analyzed by liquid chromatography-mass spectrometry

(LC-MS/MS). I manually added the sequence of human a-synuclein (SNCA) to mouse protein database of Proteome Discover Ver.2.2 (PD2.2, Thermo Scientific) and identified proteins from peptide spectra and abundances (label free quantification) (Shalit et al., 2015). For proteomic analysis, abundances of proteins were normalized based on the maximum amount of total peptide in samples. I further performed LC-MS/MS analysis two times for each hemisphere (ipsilateral side (ips) 1, ips2, contralateral side (co) 1 and co2) and compared ips1 with co1 and ips2 with co2 to define enriched proteins in ips or co that were calculated by the ratio of log2 values of co and ips (log_2co/ips).

2.10. Immunohistochemistry

The mouse brains inoculated with QD-a-syn PFFs to unilateral striatum were perfused at 6 h post injection with PBS followed by fixation with 4 % paraformaldehyde in PBS. The brains were dissected and subjected to post fixation with 4 % paraformaldehyde in PBS overnight. The brains were transferred to 0.1 M Glycine in PBS for 1 h and further immersed with sucrose solution including 30 % (w/v) sucrose and 0.05 % NaN3 in 0.1 M phosphate buffer (pH 7.2) (Wang et al., 2010) overnight. Then the brains were embedded into OCT compound and immediately frozen with liquid nitrogen. The frozen brain samples were stored at -80 °C. 20-µm-thick frozen sections were obtained with a Leica

CM1850 Cryostat (Leica Biosystems). Prior to immunostaining, the sections were incubated in Blocking One Histo (Nacalai) for blocking the nonspecific binding of antibodies. Then, the sections were incubated with primary antibodies (dilution 1:500) in dilution buffer [0.01 M phosphate buffer (pH 7.2), 0.5 M NaCl, 3 % bovine serum albumin, 5 % normal goat serum, 0.3 % Triton-x100 and 0.05 % NaN3] at 4 °C overnight, washed with PBS and labeled with secondary antibody (dilution 1:500) at room temperature for 2 h (Wang et al., 2010). The sections were washed with PBS and sealed with VECTASHIELD (H-1200, Vector Laboratories).

For immunohistochemistry of QD-a-syn PFFs, 2 µl of QD-a-syn PFFs (5 µg/µl) and a-syn PFFs (5 µg/µl) were smeared on a glass slide and fixed with 4 % paraformaldehyde in PBS for 20 min. The fixed proteins were incubated in Blocking One Histo (Nacalai), reacted with primary antibodies and secondary antibody and mounted with 50 % glycerol in PBS. These samples were observed with KEYENCE BZ-X710 fluorescence microscope equipped with the sectioning algorithm system to capture clear images without fluorescence blurring (Tanei et al., 2019) and analyzed by BZ-X Analyzer.

2.11. Data analysis

For comparison among the sample groups, data were analyzed by one-way ANOVA followed by Tukey post-test. I considered the difference between comparisons to be significant when $p < 0.05$. For bioinformatics analysis by Gene ontology and Reactome, Bonferroni adjusted p-values were calculated by DAVID functional annotation clustering website, https://david.ncifcrf.gov and Reactome Knowledgebase, https://reactome.org respectively.

Chapter 3. Results

3.1. The detection of QD-a-syn PFFs by immunostaining

First, to examine whether human a-syn PFFs can be labeled with QD, I immunostained human a-syn PFFs and QD-a-syn PFFs spotted on a glass slide with anti-Human-a-syn antibody and successfully detected QD positive dots without nonspecific signals in a-syn PFFs (Figure. 2). By counting the number of positive signals, I calculated the ratio of QD-a-syn PFFs colocalized with human a-syn PFFs to total human a-syn PFFs. The numbers of positive signals for total human a-syn PFFs was 542 and for colocalized QD-a-syn PFFs was 510, resulting that 94.1 % of total human a-syn PFFs were labeled

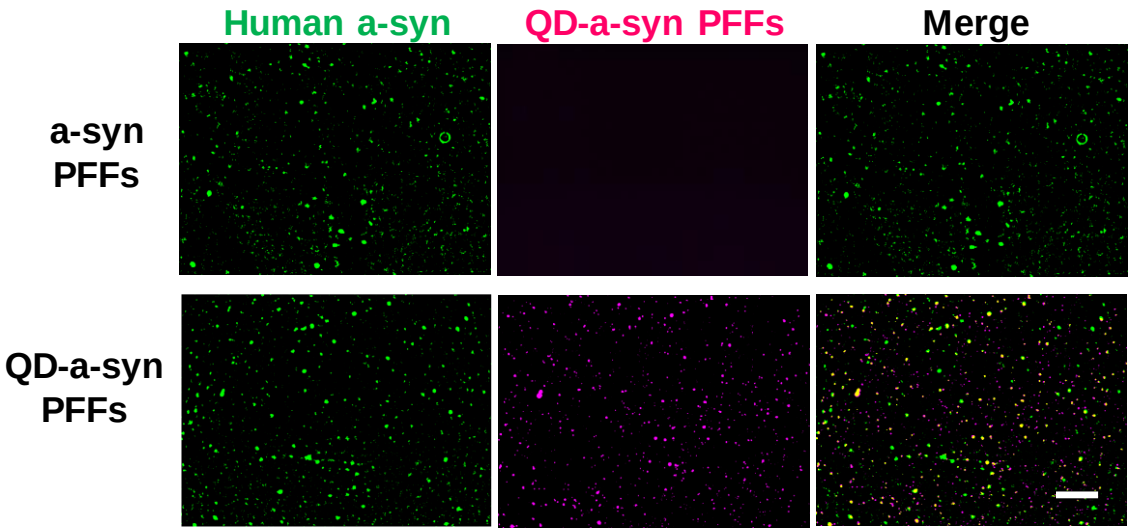

Figure. 2 Immunostaining of human a-syn PFFs or QD-a-syn PFFs using anti-Human a-syn. Human-a-syn PFFs or QD-a-syn PFFs (magenta) were spotted on a glass slide and immunostained using anti-Human-a-syn antibody (green). Merged proteins were indicated with yellow color. The numbers of positive signals per area of view (0.098 mm^2) for total human-a-syn PFFs and merged proteins were 542 and 510, respectively. Scale bar = 50 μm.

with QD. These results indicate that human a-syn PFFs were labeled with QD in a reliable manner.

3.2. Subcellular fractionation of mouse brain inoculated with QD-a-syn PFFs

To examine the subcellular localization of QD-a-syn PFFs in mouse brains at an early phase of dissemination, I injected QD-a-syn PFFs into the mouse striatum and extracted the brain at 6 hours after the injection. (Figure. 3).

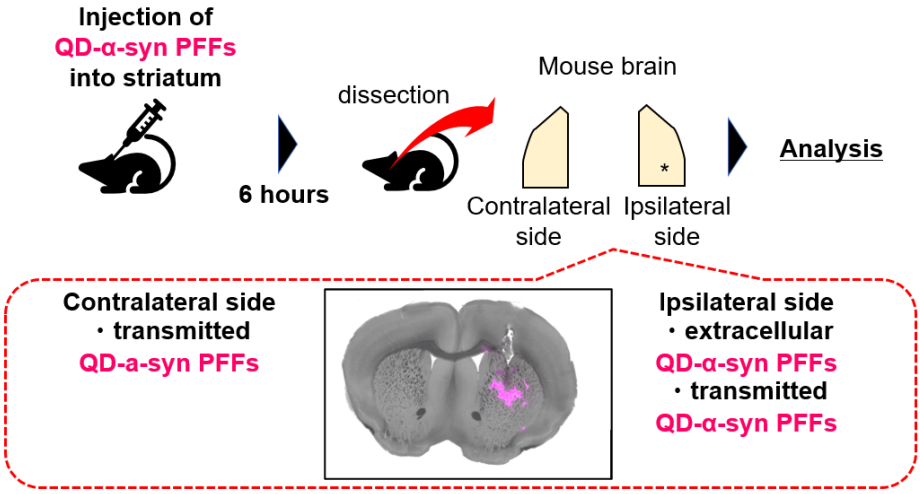

Figure. 3 Methods of the analysis of QD-a-syn injection

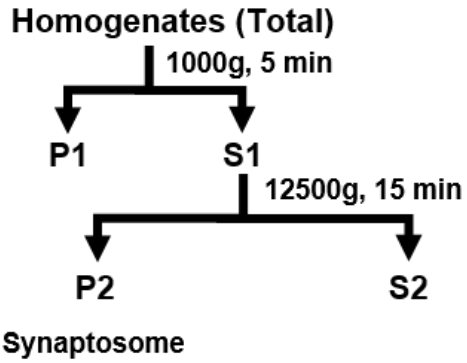

Figure. 4 Schematic description of subcellular fractionation of homogenates.

The ipsilateral or contralateral sides of brain were homogenized in 8 % sucrose buffer and applied to the subcellular fractionation.

Next, I performed subcellular fractionation of QD-a-syn PFFs-injected mouse brain homogenates based on a previous report (Kahle et al., 2000) (Figure. 4) to investigate the subcellular localization of QD-a-syn PFFs and identify the cellular components that localize to the QD-a-syn enriched fraction. As a result, particles positive for QD-a-syn

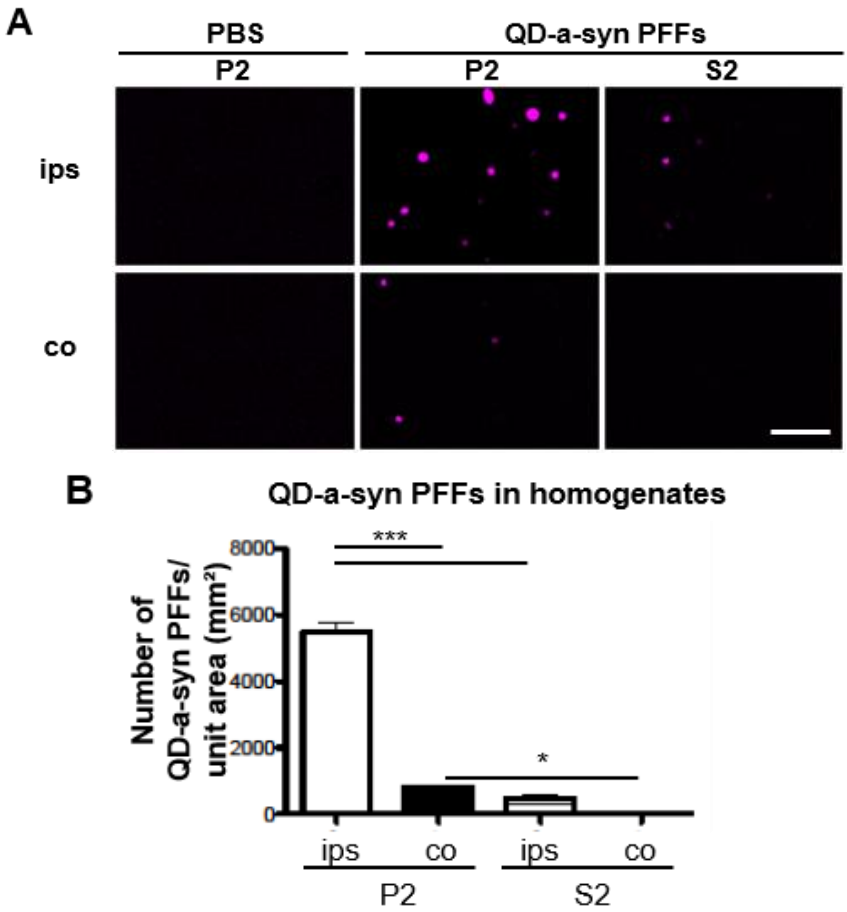

Figure. 5 Subcellular localization of QD-a-syn PFFs in mouse brain.

Smears of the P2 and S2 fraction derived from PBS- or QD-a-syn PFFs-injected brain were observed with fluorescence microscope. Scale bar = 10 μm. QD-a-syn PFFs were detected as magenta dots (A). The numbers of QD-a-syn PFFs per unit area was counted in each fraction (n = 4). Horizontal axis: fractions obtained by subcellular fractionation; vertical axis: the numbers of QD-a-syn PFFs per unit area (mm²) (B). Bars represent mean ± SD of measurements from 4 independent samples. (*$p < 0.05$, ***$p < 0.001$).

PFFs were mainly observed in the P2 fraction derived from both ipsilateral and contralateral sides of the injected hemisphere (Figure. 5A), and the numbers of QD-a-syn PFFs positive dots was larger in the P2 fraction than in the S2 fraction (Figure. 5B).

I also checked the localization of several synaptic marker proteins such as Synapsin-1 and PSD-95 in each fraction to verify the fractionation and found that these synaptic marker proteins were enriched in the P2 fraction (Figure. 6). In addition, endogenous mouse a-syn localized equally both in the P2 and S2 fractions, and P-syn was not detected in all fractions (data not shown). These results suggest that after the inoculation of QD-a-syn PFFs, exogenous QD-a-syn PFFs were enriched in the crude synaptosome fraction derived from both hemispheres at the early phase of dissemination.

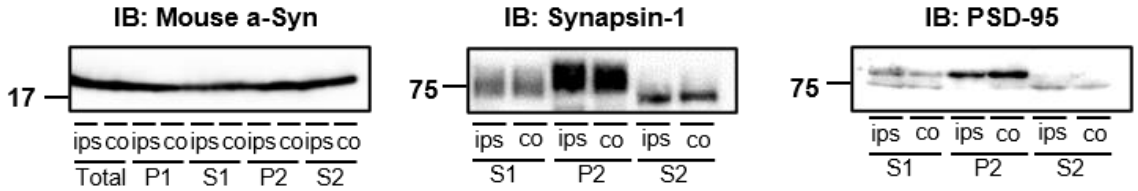

Figure. 6 Western blot analysis to detect mouse a-syn and synaptosome marker proteins.
The western blot of each fraction stained with antibodies to mouse a-syn and synaptosome markers (Synapsin-1 and PSD-95). Each experiment was performed twice.

3.3. Purification of QD-positive particles with FACS

To identify the subcellular distribution of QD-a-syn PFFs in cells, I purified QD-positive particles from P2 fraction with fluorescence-activated organelle sorting (FAOS)

by using cell sorter. QD-positive particles obtained by FAOS without any detergent are assumed to include either only QD-a-syn PFFs, particles with QD-a-syn PFFs inside or outside of the membrane structures, or complexes formed by QD-a-syn with other proteins. Based on the threshold obtained from PBS-inoculated mouse brain homogenates, I isolated QD-positive particles from the P2 fraction from the injected mouse brains (Figure. 7A). Cell sorter recognizes the QD-positive particles by forward scatter (FSC), an index of size of particles, and back scatter (BSC), an index of complexity within the particles. By analyzing 10,000 particles, I found that the QD-positive particles in the contralateral sides are smaller in size and have lower complexity than those in the ipsilateral sides (Figure. 7B). I also confirmed the isolation of QD-positive particles with fluorescence microscopy (Figure. 7C).

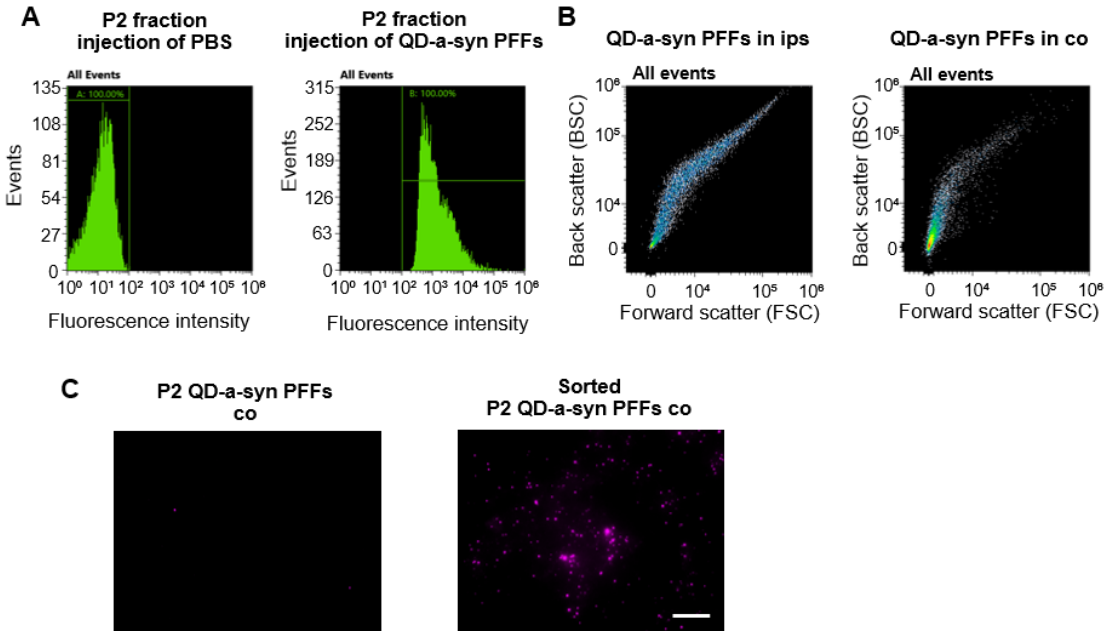

Figure. 7 Isolation of QD-a-syn PFFs-containing particles in P2 fraction with FAOS.

FAOS analysis for QD-negative particles from PBS-inoculated mouse brain homogenate and QD-positive particles from QD-a-syn PFFs-inoculated mouse brain homogenate. The sorting results of 10,000 events are shown with fluorescence intensity (A). QD-a-syn PFFs in P2 fraction were sorted by cell sorter. Cell sorter sorted 10,000 events from P2 fraction, and the sorting results were shown with back scatter (BSC) and forward scatter (FSC) (B). After the sorting (right), concentrated QD-a-syn PFFs (magenta) were validated with fluorescence microscope compared with the sample before sorting (left) (C). ips: ipsilateral side; co: contralateral side. Scale bar = 30 μm

3.4. Proteomic analysis of QD-a-syn PFFs-containing compartments

For proteomic analysis, 50,000 particles including QD-a-syn PFFs from each hemisphere were used for LC-MS/MS. The amount of QD-a-syn PFFs in P2 fraction of the ipsilateral side was 486,728 particles per 1 µg of proteins and that of the contralateral side was 70,695 particles per 1 µg of proteins, suggesting that the abundance of QD-positive organelles in the ipsilateral and contralateral sides was significantly different. Thus, I collected the P2 fractions from 2 to 3 ipsilateral or 5 to 8 contralateral hemispheres to obtain enough amount of particles. After isolating QD-positive particles with FAOS, I applied those sorted QD-positive particles to LC-MS/MS analysis (Figure. 8).

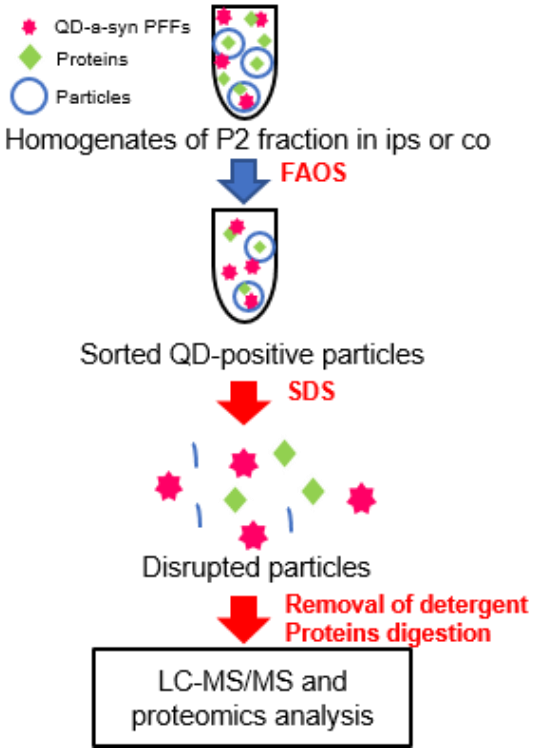

Figure. 8 Scheme of the method for proteomic analysis of QD-positive particles in the P2 fraction.

QD-positive particles underwent ultracentrifugation and treatment with SDS. After eliminating SDS with FASP, the proteins were digested with trypsin and subjected to LC-MS/MS analysis. Proteins were then identified by Proteome Discoverer (Ver.2.2) based on peptide spectra and abundances (label free quantification) (Shalit et al., 2015), and the protein abundances were normalized based on total peptide quantity. I obtained two sets of data derived from the ipsilateral and contralateral sides and compared them by their log2 values of abundance. Pearson's product correlation coefficient showed strong positive correlation, yet the value was less than 1 (Figure. 9). This indicates that some proteins were differentially expressed between the ipsilateral and the contralateral sides.

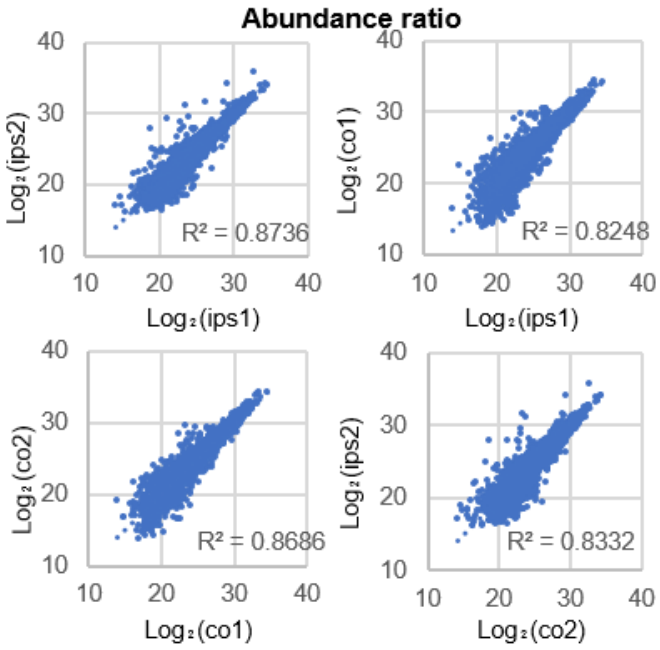

Figure. 9 Proteomic analysis of QD-positive particles in the P2 fraction.
Pearson's correlation between samples was calculated.

Based on the value of log_2co/ips, I identified 484 and 1406 proteins enriched in the ipsilateral and contralateral side respectively and 900 proteins as common proteins (Figure. 10A). These proteins identified from QD-positive particles could be associated with the intracellular compartments where QD-a-syn PFFs localized. To reveal the location and function of QD-a-syn PFFs enriched particles, I performed proteomic data analysis. DAVID bioinformatics resources consists of an integrated biological knowledgebase and analytic tools aimed at systematically extracting biological meaning from protein lists (Huang da et al., 2009). By using DAVID, I performed Gene Ontology

(GO) analysis to reveal the location of proteins detected by LC-MS/MS (Figure. 10B). GO analysis showed that the proteins in the contralateral side (log2 ratio > 1) were located in the components of neurons such as synapse, axon, dendrite and synaptic vesicle. In contrast, the proteins in the ipsilateral side (-1 > log2 ratio) were located in ribosome and ER, indicating that enriched proteins in the ipsilateral and contralateral sides have different distributions. Exosome and mitochondrion were detected from both ipsilateral and contralateral sides. GO analysis of the enriched proteins also showed that ribosomal proteins were specifically detected in the ipsilateral side (Figure. 11A and Table 1). On the other hand, neuronal and synaptic proteins were enriched in contralateral side (Figure. 11B and Table 1), suggesting that QD-a-syn PFFs are distributed in different cellular components in the ipsilateral and contralateral sides.

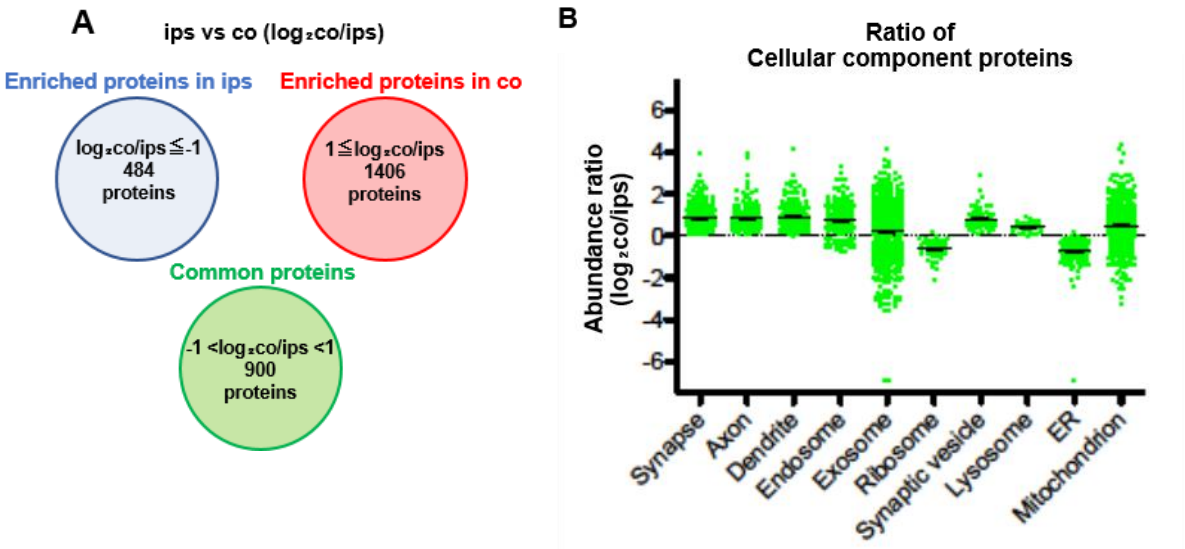

Figure. 10 Grouped the proteins detected by LC-MS/MS and the results of GO analysis for the proteins.

Based on log2 values of abundance ratio of each detected proteins, the proteins were divided into three groups: 'Enriched proteins in the ipsilateral side (ips)', 'Enriched proteins in the contralateral side (co)' and 'Common proteins' (A). GO analysis of all proteins revealed cellular component proteins, and the abundance ratio of these proteins were plotted with detected components (B).

A

Gene ontology analysis (Top 5 annotation)

Enriched proteins in ips

Biological Process

Term	Count	Bonferroni
cellular amide metabolic process	61	7.38E-08
peptide metabolic process	55	7.65E-08
oxidation-reduction process	57	9.24E-08
translation	48	2.33E-07
mitochondrion organization	46	4.28E-07

Cellular Component

Term	Count	Bonferroni
mitochondrion	129	8.50E-21
mitochondrial part	76	3.93E-15
extracellular exosome	146	1.12E-12
extracellular vesicle	146	1.82E-12
membrane-bounded vesicle	173	2.10E-12

B

Enriched proteins in co

Biological Process

Term	Count	Bonferroni
anterograde trans-synaptic signaling	119	3.21E-24
trans-synaptic signaling	119	3.21E-24
synaptic signaling	119	3.21E-24
chemical synaptic transmission	119	3.21E-24
cellular localization	294	1.30E-23

Cellular Component

Term	Count	Bonferroni
synapse	205	2.53E-40
neuron part	295	3.98E-37
synapse part	170	4.60E-35
neuron projection	236	9.10E-31
membrane-bounded vesicle	465	6.98E-27

Figure. 11 Gene ontology analysis of enriched proteins.

Enriched proteins were applied for GO analysis and top 5 terms in order of p values are shown (A and B). All results of GO analysis are also shown in Table 1.

I further analyzed the enriched proteins with Reactome (Jassal et al., 2020) and revealed that specific patterns of biological pathways in each hemisphere correlated with the results of GO analysis (Figure. 12A). These analyses notably showed that QD-a-syn PFFs in the ipsilateral side localized in the compartments associated with ER. Alternatively, QD-a-syn PFFs in the contralateral side, most of which were transmitted from the ipsilateral side, localized in the compartments associated with synapses. More specifically, Reactome pathways (p-value = 0.05) shown in the heat map (Figure. 12B) indicated that most enriched proteins in the ipsilateral side are implicated in metabolism of protein and translation. On the other hand, the enriched proteins in the contralateral side are implicated in the neuronal system such as neuronal transmitter release, activation of NMDA receptors and vesicle-mediated transport including clathrin-mediated endocytosis and Golgi-to-ER retrograde transport.

A

Reactome (Top 5 terms)

ips

Pathway name	Count	pValue
The citric acid (TCA) cycle and respiratory electron transport	46	1.11E-16
Respiratory electron transport, ATP synthesis by chemiosmotic coupling, and heat production by uncoupling proteins.	31	9.76E-14
SRP-dependent cotranslational protein targeting to membrane	26	2.92E-12
Translation	44	5.23E-12
Eukaryotic Translation Elongation	23	2.86E-11

co

Pathway name	Count	pValue
Neuronal System	117	1.14E-14
Neurotransmitter receptors and postsynaptic signal transmission	63	7.43E-11
Transmission across Chemical Synapses	83	7.77E-11
Activation of NMDA receptors and postsynaptic events	37	7.59E-09
Cooperation of PDCL (PhLP1) and TRiC/CCT in G-protein beta folding	22	9.24E-09

B

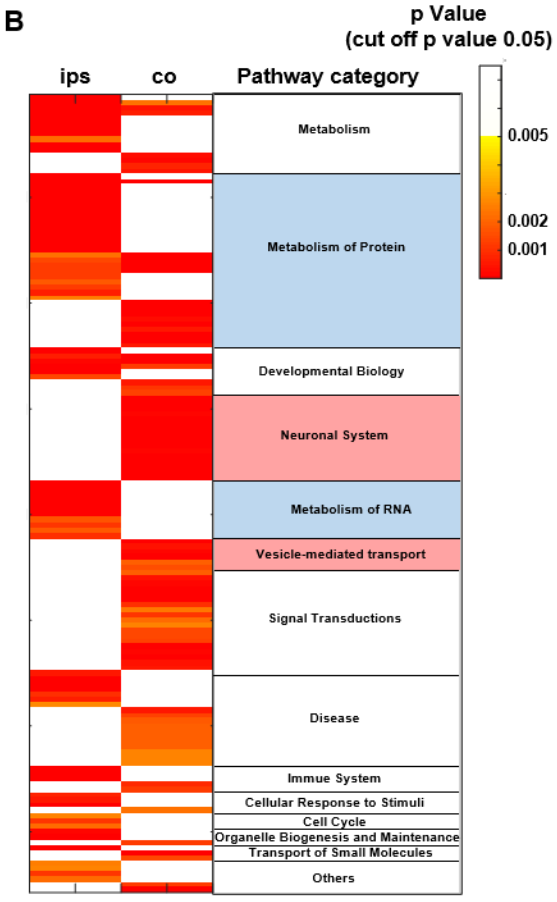

Figure. 12 Reactome analysis of enriched proteins in ips or co.

Reactome analysis of the enriched proteins revealed biological annotation (A). Pathway categories that were defined by Reactome are shown by heat map based on p-values. The pathway categories with colors are statistically significant. blue: ips; red: co (B).

3.5. Localization of QD-a-syn PFFs in the brain

To validate whether the results of distribution analysis reflect the localization of QD-a-syn PFFs in brain, I performed immunohistochemistry of several marker proteins, which were detected in proteomic analysis, using frozen sections of QD-a-syn PFFs injected mouse brain. I calculated the percentages of QD-a-syn PFFs colocalized with the markers in the striatum and cortex where QD-a-syn PFFs spread. I found that synaptic marker proteins, synapsin-1 and synaptophysin-1 that belong to 'synapse' in the result of GO analysis, colocalized more with QD-a-syn PFFs in the contralateral side than in the ipsilateral side (Figure. 13A and B). On the other hand, an ER marker protein, ERp57, colocalized with QD-a-syn PFFs more in the ipsilateral side compared to the contralateral side (Figure. 14A). These results suggest that proteomic analysis of the QD-a-syn PFFs enriched fraction reflects the localization of QD-a-syn PFFs in brain. CD81, an exosome marker protein that belongs to 'extracellular exosome' in the result of GO analysis, was detected in both sides of the brain (Table 2) but colocalized with QD-a-syn PFFs more in the contralateral side compared to the ipsilateral side (Figure. 14B). I also investigated the colocalization of QD-a-syn PFFs with a mitochondrial marker protein, Tom20, which was detected in 'mitochondrion' in the result of GO analysis. Around 50 % of QD-a-syn PFFs colocalized with Tom20 in both sides (Figure 14C). This result is highly consistent

with the result obtained in the proteomic analysis (Figure. 10B), suggesting that bilaterally transmitted QD-a-syn PFFs colocalized with mitochondria in the brain.

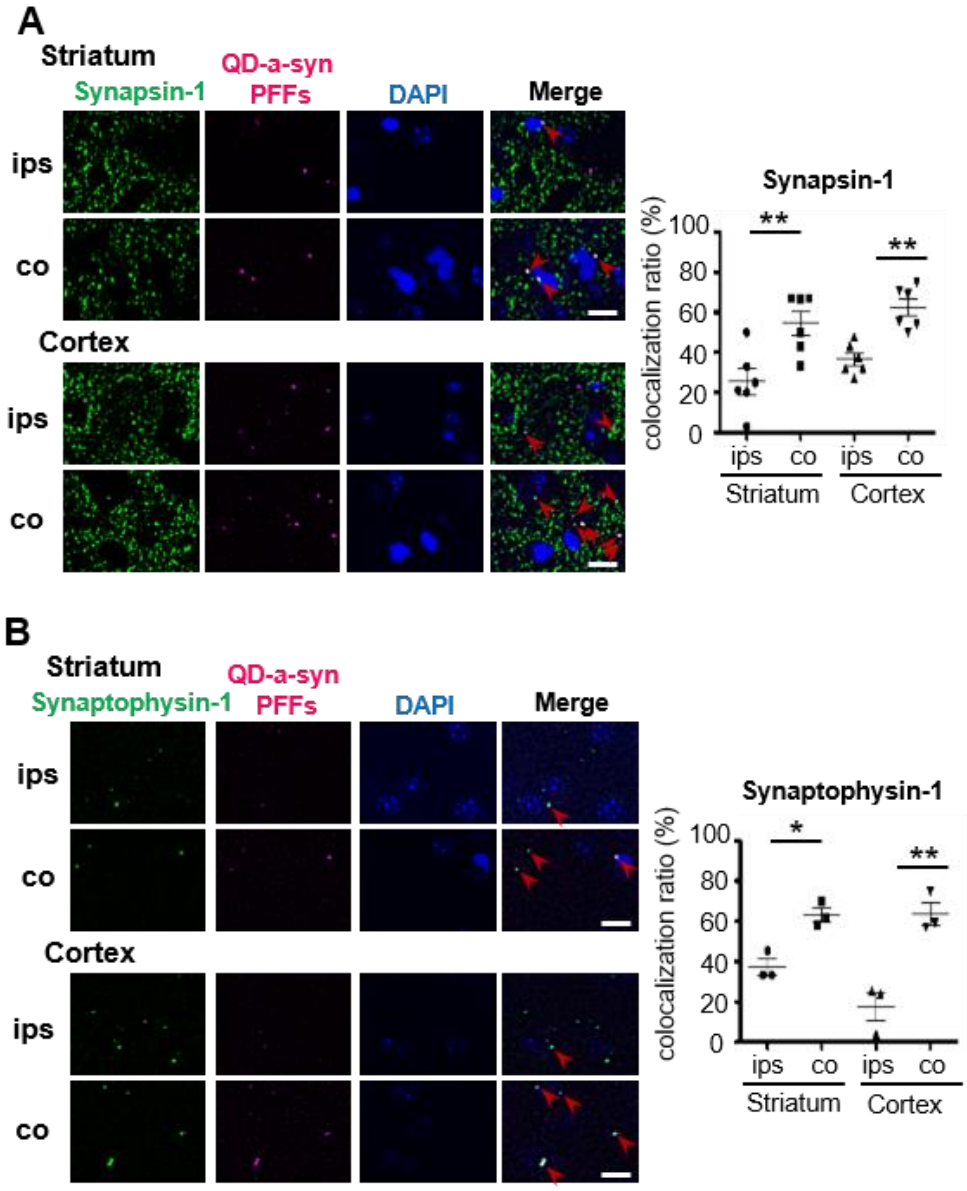

Figure. 13 Colocalization of QD-a-syn PFFs with synapses in mouse brain.

The frozen sections of mouse brains at 6 hours after the injection of QD-a-syn PFFs into the striatum were immunostained with antibodies to the indicated marker proteins Synapsin-1 (A) and Synaptophysin-1 (B) (green), which were used as synaptic marker proteins, were detected by LC-MS/MS analysis. QD-a-syn PFFs (magenta) and DAPI nuclear staining (blue) are also shown. QD-a-syn PFFs that colocalized with marker proteins are indicated by arrow heads (red). The ratio of colocalized QD-a-syn PFFs to total QD-a-syn PFFs was calculated in each region and shown in the graphs (A-B). Scale bar = 10 μm. Bars in graphs represent mean ± SD of measurements from 3 to 6 independent samples (*$p < 0.05$, **$p < 0.01$). ips: ipsilateral side, co: contralateral side.

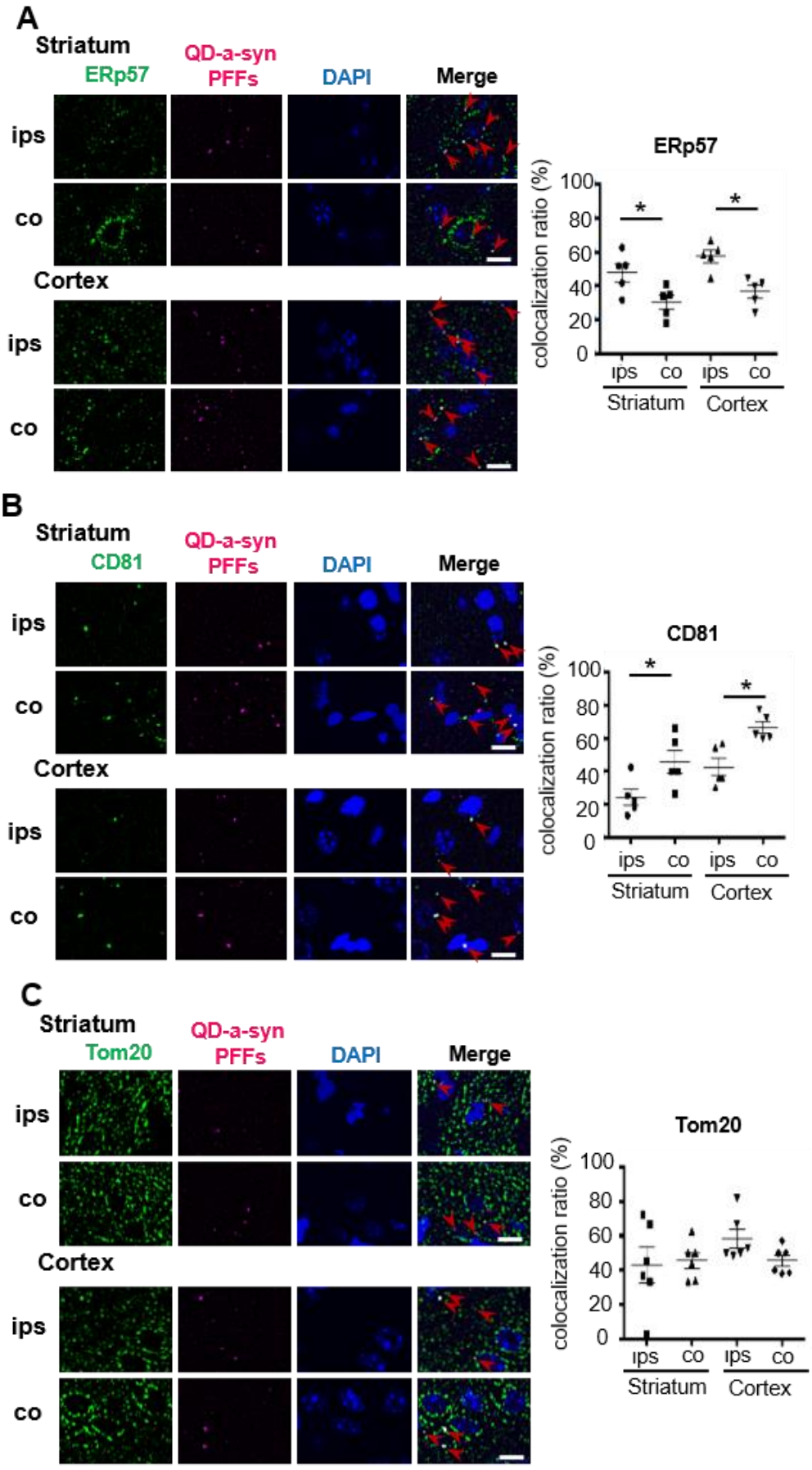
A
Striatum
ERp57
QD-a-syn PFFs
DAPI
Merge
ips
co
Cortex
ips
co
ERp57
colocalization ratio (%)
100
80
60
40
20
0
*
*
ips
co
ips
co
Striatum
Cortex
B
Striatum
CD81
QD-a-syn PFFs
DAPI
Merge
ips
co
Cortex
ips
co
CD81
colocalization ratio (%)
100
80
60
40
20
0
*
*
ips
co
ips
co
Striatum
Cortex
C
Striatum
Tom20
QD-a-syn PFFs
DAPI
Merge
ips
co
Cortex
ips
co
Tom20
colocalization ratio (%)
100
80
60
40
20
0
ips
co
ips
co
Striatum
Cortex

Figure. 14 Colocalization of QD-a-syn PFFs with cellular organelles in mouse brain.
The frozen sections of mouse brains at 6 hours after the injection of QD-a-syn PFFs into striatum were immunostained with antibodies to the indicated marker proteins. ERp57 (A), CD81 (B), Tom20 (C), which were used as marker proteins for ER, exosome and mitochondria (green), were detected by LC-MS/MS analysis. QD-a-syn PFFs (magenta) and DAPI nuclear staining (blue) are also shown. QD-a-syn PFFs that colocalized with marker proteins are indicated by arrow heads (red). The ratio of colocalized QD-a-syn PFFs to total QD-a-syn PFFs was calculated in each region and shown in the graphs (A-C). Scale bar = 10 μm. Bars in graphs represent mean ± SD of measurements from 5 to 6 independent samples (*p< 0.05, **p< 0.01). Ips: ipsilateral side, co: contralateral side.

Moreover, to confirm whether the a-syn PFFs localize in microglia, Iba-1, a microglial marker protein, was immunostained. As a result, Iba-1 colocalized with around 30 % of QD-a-syn PFFs in both sides (Figure. 15). This result suggests that microglia might be involved in the transmission at the early phase. Taken together, proteomic analysis of QD-a-syn PFFs enriched fraction reflects the subcellular compartments in which the PFFs disseminated during the early phase of QD-a-syn PFFs transmission.

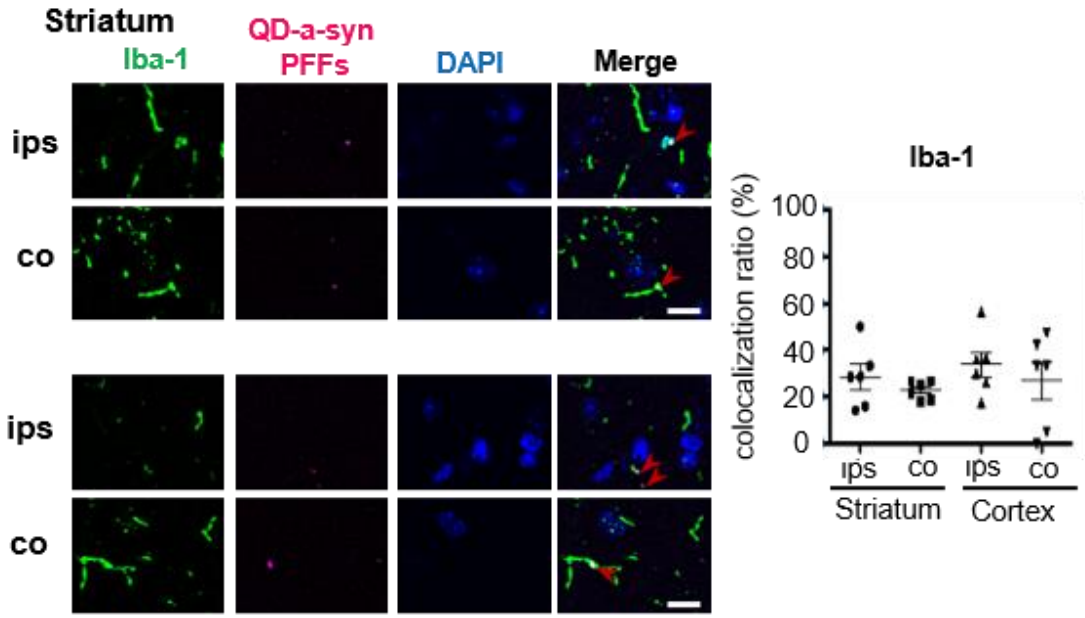

Figure. 15 Colocalization of QD-a-syn PFFs with microglia in mouse brain.

The frozen sections of mouse brains at 6 hours after the injection of QD-a-syn PFFs into striatum were immunostained with antibodies to the indicated marker proteins. Iba-1, which was used as a microglial marker protein (green), were detected by LC-MS/MS analysis. QD-a-syn PFFs (magenta) and DAPI nuclear staining (blue) are also shown. QD-a-syn PFFs that colocalized with marker proteins are indicated by arrow heads (red). The ratio of colocalized QD-a-syn PFFs to total QD-a-syn PFFs was calculated in each region and shown in the graphs. Scale bar = 10 μm. Bars in graphs represent mean ± SD of measurements from 6 independent samples. ips: ipsilateral side, co: contralateral side.

Chapter 4. Discussion

4.1. Rapid dissemination of QD-a-syn PFFs

Recently, many studies have confirmed that exogenous a-syn PFFs induce endogenous a-syn pathology *in vivo* (Luk et al., 2012, Giaime et al., 2017, Masuda-Suzukake et al., 2014, Henderson et al., 2019). In these studies, exogenous a-syn PFFs work as seeds of a-syn pathology and allow endogenous a-syn to accumulate as a phosphorylated form (P-syn) within from 3 weeks to 3 months after the inoculation. A previous study also showed that the accumulation of P-syn was detected from 2 to 3 months after the inoculation of the seeds. Even though the seeds were inoculated unilaterally, disseminated pathology was observed in bilateral hemispheres (Okuzumi et al., 2018). When the corpus callosum was severed before the injection, the a-syn transmission from the injected side to the contralateral hemisphere was significantly reduced. However, when the dissection was performed 1 day after the injection, the a-syn pathology of the contralateral side was recognized, suggesting that the spread of a-syn seeds can occur within a day (Okuzumi et al., 2018). In this study, to investigate the precise transmission mechanism of a-syn seeds, I explored their localizations at 6 hours post injection before the onset of pathological P-syn accumulation. I labeled the a-syn PFFs with QD to show strong fluorescence and found that a-syn PFFs were distributed in P2 fraction after the subcellular fractionation at the early phase of post-inoculation. I

further purified the particles which have QD-a-syn PFFs using organelle sorting and subjected those particles to the proteomic analysis.

4.2. Distinct protein compositions of QD-positive particles derived from each hemisphere

Cell sorter analysis revealed that QD-positive particles in the ipsilateral side had different sizes and particle complexity compared to those in the contralateral side (Figure. 7B). Based on FSC, the index of particle sizes, QD-positive particles have larger sizes in the ipsilateral side than those in the contralateral side. It is likely that homogenates in the ipsilateral side included the inoculated QD-a-syn PFFs, and homogenates in the contralateral side included transported QD-a-syn PFFs. Also, GO and Reactome analyses suggested that QD-a-syn PFFs in each hemisphere were associated with different organelles (Figure. 10B, Figure. 11 and Figure. 12). Such different localizations of QD-a-syn PFFs might determine the size and complexity of the particles.

4.3. Mechanisms underlying the broad transmission of a-syn-PFFs

A previous work suggested that inoculated a-syn PFFs were transported through the corpus callosum (Okuzumi et al., 2018), suggesting that seeds were transported from the ipsilateral side to the contralateral side through an axonal transport mechanism. GO analysis showed that enriched proteins in the contralateral side contained component

proteins of `axon` (Figure.10B and Table. 1), including anterograde transport proteins such as Ap3b2 and Kif1a. Ap3b2, a subunit of non-clathrin- and clathrin-associated adaptor protein complex 3, was involved in protein sorting and reported as one of potential PD risk genes (Bandres-Ciga et al., 2019). Kif1a is a transport component of synaptic vesicle precursor (Yonekawa et al., 1998). I also detected Dync1h1, a component of cytoplasmic dynein 1 complex in common proteins, which is known to transport retrograde cargos (Hirokawa et al., 2010). My findings and these reports suggest that axonal transport might be associated with the transmission of a-syn PFFs, however, the causal relationship between the axonal transport and the localization of QD-a-syn PFFs at synapses and ERs has not been fully investigated. Further studies should be performed in order to confirm the interaction between a-syn PFFs and proteins that mediate the axonal transport.

4.4. Is trans-synaptic transfer involved in the dissemination of a-syn-PFFs?

Proteomic analysis showed that sorted QD-positive particles included peptides derived from synaptosome, a subcellular component of the P2 fraction (Kahle et al., 2000). In the contralateral side, the synapse related proteins were mainly detected (Figure. 11 and Figure. 12). By immunohistochemical analysis, I confirmed that synapsin-1 and synaptophysin-1 colocalized with QD-a-syn PFFs, and the ratio of colocalization was

higher in the contralateral side (Figure. 13A and B). These results corresponded to that of proteomic analysis. Previously Okuzumi et al. showed that pre-injection of Botulinum toxin B, which suppresses synaptic vesicle fusion at pre-synapses, into the contralateral striatum before the inoculation of a-syn PFFs inhibited the dissemination of P-syn pathology in the contralateral hemisphere (Okuzumi et al., 2018). In this study, I detected SNAP25, a SNARE protein, which is essential for synaptic vesicle exocytosis as well as exocytosis of other secretory granules. The interaction of SNAP25 with a-syn was suggested by Ingenuity Pathway Analysis (Hernandez et al., 2020). These results suggest the involvement of the SNARE-mediated exocytosis in the dissemination process of a-syn seeds.

4.5. Hypothesis of the function of a-syn in mitochondria

The mitochondrion was within the top 5 terms of subcellular components enriched in the ipsilateral side. Immunohistochemical analysis showed that a mitochondrial protein Tom20, which was detected in proteomic analysis, colocalized with QD-a-syn PFFs. However, the ratio of colocalization was not different between both sides of the brain (Figure. 14C). This might be due to the existence of neuronal function-related proteins in the contralateral side. Several reports suggested that a-syn promotes oxidative stress (Hsu et al., 2000), and a-syn PFFs induces synaptic dysfunction such as decreases

in synaptic protein expression and the reduction of amplitudes of Ca^{2+} transient in primary neurons (Froula et al., 2018, Volpicelli-Daley et al., 2011, Bridi and Hirth, 2018) as well as mitochondrial disfunction (Gribaudo et al., 2019). In addition, a-syn interacts with Tom20 in human dopaminergic neurons from PD patients and impairs the mitochondrial protein import *in vitro* (Di Maio et al., 2016). These reports and the results in this study suggest that a-syn seeds as well as a-syn itself might interact with mitochondria.

4.6. Transmission mechanism through exosomes

Exosomes contain various proteins and mRNA derived from released cells and play a role in cell-to-cell communication. In central nervous systems, most cell types can release exosomes, including neurons and glial cells (Von Bartheld and Altick, 2011).

Studies have shown that primary-cultured microglia treated with a-syn PFFs release exosomes with misfolded a-syn within 24 hours (Guo et al., 2020) and neuron-derived exosomes containing fibrillar a-syn and ubiquitinated proteins, thus accelerating the transmission of pathological a-syn among neurons (Russo et al., 2012). Interestingly, extracellular exosome in GO term was detected by proteomic analysis in both hemispheres (Table 1). The immunohistochemical analysis allowed us to confirm that QD-a-syn PFFs and CD81, an exosome marker, colocalized in both sides of the brain

(Figure. 14B). These results suggest that QD-a-syn PFFs could be exported from cells by exosomes, which contributes to the transmission of a-syn seeds.

In this study, I found that although extracellular exosomes were detected in enriched proteins in both hemispheres (Figure.10B), the colocalization ratio between exosomes and QD-a-syn PFFs was significantly higher in the contralateral side compared to the ipsilateral side (Figure.14B). To understand the features of exosomes in each hemisphere, I additionally analyzed the proteins belonging to ‘extracellular exosome’ in each hemisphere by STRING (v11), a biological database of protein-protein interactions and found that the most of exosome proteins were involved in keratinocyte differentiation, ribosome, and spliceosome (Figure. 16). However, exosome proteins in the contralateral side were involved in the chaperone-mediated protein folding, proteasome, and transmission across chemical synapses (Figure. 17). STRING analysis suggests that exosomes in the contralateral side are highly associated with synapses than the ipsilateral side, and this association might affect the colocalization ratio between QD-a-syn PFFs and exosomes.

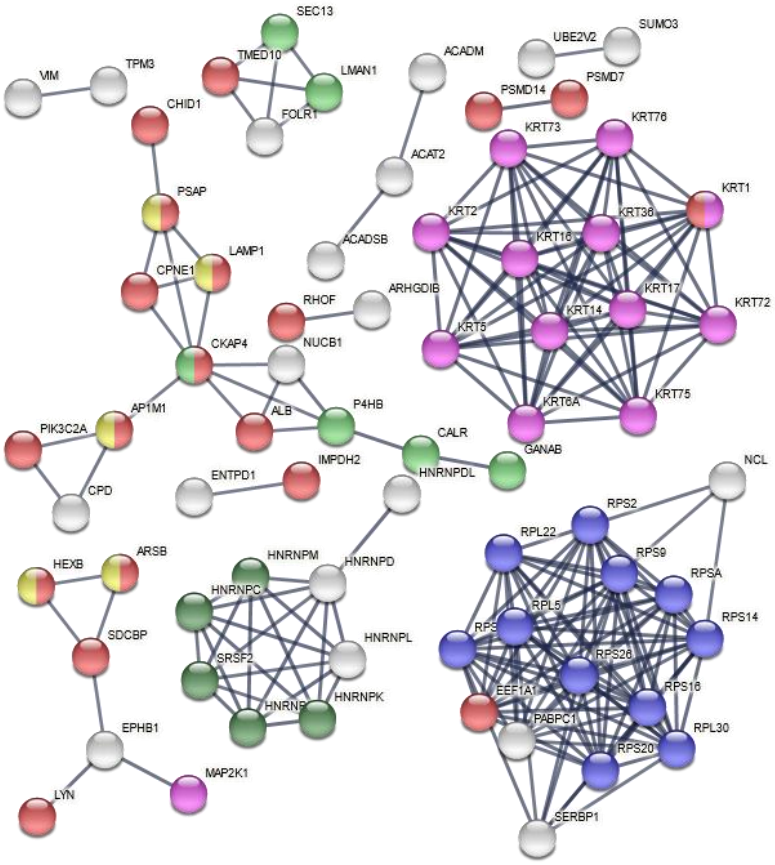

Term	p value
Keratinocyte differentiation	4.43E-07
Exocytosis	5.21E-07
Ribosome	2.31E-07
Protein processing in endoplasmic reticulum	0.004
Lysosome	0.0045
Spliceosome	0.0242

Figure. 16 STRING analysis of enriched proteins belonging to 'extracellular exosome' in ips.
The proteins in ips were analyzed by STRING and STRING interaction maps are shown. Selected significantly enriched terms of KEGG, GO and Reactome are displayed.

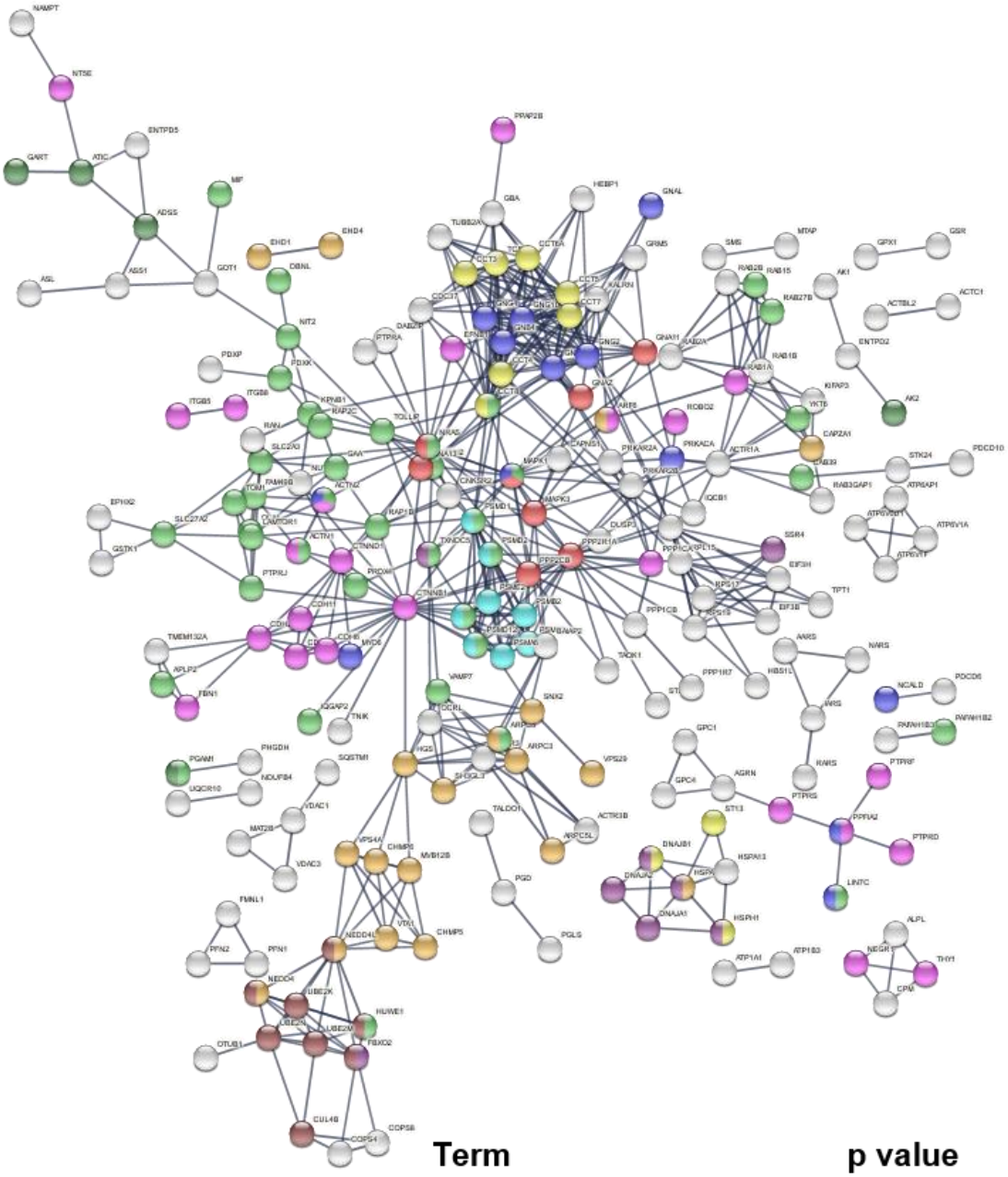

Term	p value
Chaperone-mediated protein folding	4.16E-05
Exocytosis	5.11E-11
Biological adhesion	0.00021
Ribonucleotide biosynthetic process	0.0084
Proteasome	0.00017
Endocytosis	3.88E-06
Long-term depression	0.0007
Protein processing in endoplasmic reticulum	0.0217
Ubiquitin mediated proteolysis	0.225
Transmission across Chemical synapses	8.65E-05

Figure. 17 STRING analysis of enriched proteins belonging to 'extracellular exosome' in co.

The proteins were analyzed by STRING and STRING interaction maps are shown. Selected significantly enriched terms of KEGG, GO and Reactome are displayed.

4.7. A-syn PFFs in ER and vesicular trafficking

Several internalization mechanisms of the a-syn fibrils have been proposed including dynamin-mediated endocytosis (Lee et al., 2008) or cell surface protein-mediated uptake such as heparan sulfate proteoglycan (Holmes et al., 2013) and LAG3 (Mao et al., 2016). In this study, I assumed that a-syn PFFs are internalized in the ipsilateral side and transported into the contralateral side. However, my proteomic analysis showed that component proteins belonging to endosomes were enriched in the contralateral side (Figure.10B), and the proteins related to vesicle-mediated transport was significantly found in the contralateral side (Figure.12B). According to previous studies, exosomes are internalized into cells through endocytosis (Chivet et al., 2014, Gonda et al., 2019), and in this study, I confirmed that the component proteins of exosomes were significantly found in the contralateral side (Figure.14B). Also, Cooper et al. reported that the accumulation of pathological a-syn blocks ER to Golgi vesicular trafficking, and overexpression of Rab1, which regulates ER to Golgi protein trafficking, reduces the accumulation of pathological a-syn in ER (Cooper et al., 2006). This report suggests that cells export pathological a-syn from ER, and its trafficking might be suppressed by accumulation of a-syn. In the current study, I showed that component proteins of ER were enriched in the ipsilateral side (Figure.10B). The immunohistochemical analysis suggested that the ER marker protein, ERp57, colocalized with QD-a-syn PFFs more in

the ipsilateral side compared to the contralateral side. Thus, in the ipsilateral side, QD-a-syn PFFs could be released from ER or accumulated in ER blocking the ER to Golgi vesicular trafficking, whereas vesicle-mediated endocytosis could be activated by the internalization of exosomes as reflected in the results of my proteomic analysis.

4.8. Roles of microglia in the a-syn transmission

I further performed immunohistochemistry of Iba-1, a marker for microglia (Figure. 15). Recently, George et al. reported that microglia modulates the cell to cell transfer of a-syn under resting, non-inflammatory conditions (George et al., 2019), which might be related to the colocalization of QD-a-syn PFFs and a microglial marker protein observed in this study. Also, they suggested that microglia can efficiently engulf extracellular a-syn aggregates (George and Brundin, 2015), which indicate that the colocalization ratio of QD-a-syn PFFs and microglia can be higher in the ipsilateral side than in the contralateral side. However, microglia colocalized with approximately 30 % of QD-a-syn PFFs with no significant differences between the ipsilateral and contralateral sides (Figure. 15). The images captured in the cortex and striatum outside the injection site where QD-a-syn PFFs largely remained explains this lack of significant differences.

4.9. Conclusions and future perspectives

In this study, I showed that a-syn PFFs transmitted through the mouse brain localized to the ER, synapses, exosomes, mitochondria and microglia, and revealed the candidate proteins responsible for initial transmission of pathological a-syn before the onset of a-syn pathology. The results suggest two plausible hypotheses – either these components and proteins contribute to the transmission of a-syn seeds or are directly involved in the accumulation of a-syn seeds.

A-syn PFFs internalized into cells in the ipsilateral side colocalized with the ER, while a-syn PFFs transmitted to the contralateral side colocalized with synapses and exosomes. Since this study mainly focused on the subcellular components in which QD-a-syn PFFs localized, it remains to be determined which cell types and the molecules are involved in the transmission of a-syn PFFs. I propose experiments that may help elucidate the transmission of a-syn PFFs by each cell type - the injection of QD-a-syn PFFs using mice expressing fluorescent proteins in various cell types such as neurons, microglia and astrocytes, and then sorting each cell type expressing fluorescent proteins.

To narrow down the molecules directly involved in the a-syn transmission, QD-positive particles obtained from mouse brain homogenates could be treated with detergents prior to isolation of QD-positive particles by cell sorter. Since the obtained

proteins complex with QD-a-syn PFFs directly, proteomic analysis of these proteins can be used to identify the molecules that are important for the transmission of a-syn seeds. Also, genetic knockdown/knockout approaches can be available to evaluate the impact of the candidate molecules.

To date, how pathological a-syn spreads in the brains of PD has not been elucidated, and still no effective therapeutic agents to suppress the spread of pathological a-syn is available. Further investigations as described above are expected to identify the proteins and pathways related to the transmission of pathological a-syn, and targeting the identified proteins or pathways to prevent the pathological a-syn from spreading in the disease brain may be an effective therapeutic strategy for PD.

Table 1 GO analysis of enriched proteins.

Enriched proteins in ips	
Biological process	
Term	Bonferroni
cellular amide metabolic process	7.37814E-08
peptide metabolic process	7.64763E-08
oxidation-reduction process	9.24296E-08
translation	2.32814E-07
mitochondrion organization	4.27834E-07
peptide biosynthetic process	6.1687E-07
intermediate filament cytoskeleton organization	1.33501E-06
intermediate filament-based process	1.7564E-06
amide biosynthetic process	1.26327E-05
intermediate filament organization	0.000312387
organonitrogen compound biosynthetic process	0.00270317
generation of precursor metabolites and energy	0.003102185
electron transport chain	0.005424233
cellular respiration	0.010122033
energy derivation by oxidation of organic compounds	0.010343477
cellular response to stress	0.034572896
mitochondrial ATP synthesis coupled electron transport	0.040613808
intracellular transport	0.051098873
single-organism organelle organization	0.052992076
cellular macromolecular complex assembly	0.053043816
macromolecular complex assembly	0.055778222

Enriched proteins in ips	
Cellular component	
Term	Bonferroni
mitochondrion	8.49911E-21
mitochondrial part	3.92774E-15
extracellular exosome	1.12266E-12
extracellular vesicle	1.82432E-12
membrane-bounded vesicle	2.10498E-12
extracellular organelle	2.31548E-12
organelle envelope	9.43804E-10
envelope	1.18125E-09
organelle inner membrane	3.29233E-09
mitochondrial protein complex	2.73466E-08
mitochondrial membrane	5.12325E-08
mitochondrial inner membrane	6.24756E-08
mitochondrial envelope	6.28271E-08
intermediate filament	7.18888E-07
ribosome	7.57778E-07
endoplasmic reticulum	1.1317E-06
inner mitochondrial membrane protein complex	1.86635E-06
mitochondrial membrane part	2.29533E-06
ribosomal subunit	2.53851E-06
small ribosomal subunit	1.04409E-05
intermediate filament cytoskeleton	1.09476E-05
mitochondrial matrix	1.43796E-05
cytosolic small ribosomal subunit	1.78494E-05
intracellular ribonucleoprotein complex	4.6285E-05
ribonucleoprotein complex	4.79776E-05
endoplasmic reticulum part	5.20566E-05
oxidoreductase complex	0.000133561
nuclear outer membrane-endoplasmic reticulum membrane network	0.000263275
extracellular region part	0.000281456
mitochondrial respiratory chain	0.000298566
endoplasmic reticulum membrane	0.000726517
respiratory chain	0.000920971
cytosolic ribosome	0.001422629
respiratory chain complex	0.001728884
cytosolic part	0.003011752
extracellular matrix	0.005755707

myelin sheath	0.010058586
NADH dehydrogenase complex	0.034457139
mitochondrial respiratory chain complex I	0.034457139
respiratory chain complex I	0.034457139

Enriched protein in co	
Biological process	
Term	Bonferroni
anterograde trans-synaptic signaling	3.2078E-24
trans-synaptic signaling	3.2078E-24
synaptic signaling	3.2078E-24
chemical synaptic transmission	3.2078E-24
cellular localization	1.2998E-23
protein localization	7.68741E-21
vesicle-mediated transport	4.85981E-19
modulation of synaptic transmission	6.41994E-18
cellular protein localization	4.85164E-17
cellular macromolecule localization	5.39588E-17
macromolecule localization	1.01667E-16
establishment of localization in cell	3.68677E-15
establishment of protein localization	1.0598E-14
nervous system development	2.27237E-14
regulation of synapse structure or activity	3.99871E-14
cell-cell signaling	5.25443E-14
transmembrane transport	9.48942E-14
regulation of cellular component organization	6.93046E-12
protein transport	9.24061E-12
neuron development	1.00107E-11
neurogenesis	1.38609E-11
ion transport	7.23848E-11
neuron projection development	7.6235E-11
regulation of transport	8.77858E-11
cellular component assembly	1.13968E-10
membrane organization	1.97133E-10
regulation of synaptic plasticity	5.09004E-10
exocytosis	7.80831E-10
cellular amide metabolic process	8.19334E-10
generation of neurons	8.76318E-10
organonitrogen compound biosynthetic process	1.02879E-09
cellular component biogenesis	1.5401E-09
regulation of neuronal synaptic plasticity	1.56628E-09
phosphate-containing compound metabolic process	2.05373E-09
phosphorus metabolic process	2.46801E-09
neurotransmitter transport	4.39083E-09

positive regulation of cellular component organization	4.73042E-09
peptide metabolic process	5.96404E-09
synapse organization	6.83343E-09
dendrite development	8.07552E-09
single-organism membrane organization	8.78089E-09
neuron differentiation	1.21183E-08
intracellular transport	2.87152E-08
single-organism organelle organization	2.88345E-08
cell projection organization	4.92732E-08
single-organism behavior	6.0757E-08
behavior	6.40513E-08
intracellular protein transport	9.26979E-08
protein complex subunit organization	9.4034E-08
protein complex assembly	1.64062E-07
protein complex biogenesis	1.69861E-07
learning	2.08432E-07
regulation of cell projection organization	2.34698E-07
regulation of neurotransmitter levels	2.48203E-07
single-organism cellular localization	3.56978E-07
ion transmembrane transport	3.75073E-07
regulation of neuron projection development	5.31387E-07
mitochondrion organization	7.39605E-07
macromolecular complex assembly	7.48646E-07
regulation of cellular localization	7.60903E-07
protein localization to membrane	7.90056E-07
neuron projection morphogenesis	1.11637E-06
regulation of nervous system development	2.13652E-06
amide biosynthetic process	5.03679E-06
regulation of ion transmembrane transport	6.77313E-06
endomembrane system organization	7.12521E-06
actin filament-based process	8.8272E-06
actin cytoskeleton organization	1.2075E-05
translation	1.33452E-05
peptide biosynthetic process	1.33536E-05
cell morphogenesis involved in neuron differentiation	1.33984E-05
presynaptic process involved in chemical synaptic transmission	1.37076E-05
regulation of transmembrane transport	1.46419E-05

regulation of ion transport	1.63475E-05
secretion by cell	1.964E-05
locomotory behavior	2.12255E-05
regulation of dendrite development	2.14501E-05
neurotransmitter secretion	2.16641E-05
signal release from synapse	2.16641E-05
inorganic ion transmembrane transport	2.79437E-05
dendrite morphogenesis	3.08586E-05
cellular catabolic process	3.37469E-05
regulation of neurogenesis	3.44611E-05
cognition	3.70355E-05
dephosphorylation	3.9164E-05
anion transport	3.93966E-05
regulation of vesicle-mediated transport	4.24019E-05
neuron-neuron synaptic transmission	4.56203E-05
regulation of cellular component biogenesis	7.17256E-05
regulation of signaling	9.04063E-05
vacuolar transport	0.000106484
positive regulation of synaptic transmission	0.000127527
regulation of long-term neuronal synaptic plasticity	0.000137362
regulation of cell communication	0.000151107
regulation of cell morphogenesis	0.000163654
cell part morphogenesis	0.000196745
cell projection morphogenesis	0.000197661
regulation of neuron differentiation	0.000236291
learning or memory	0.000240349
protein catabolic process	0.000298384
neuromuscular process	0.000301756
membrane docking	0.000312958
regulation of cell morphogenesis involved in differentiation	0.000434991
tRNA aminoacylation	0.000465805
organophosphate metabolic process	0.00048528
secretion	0.000645562
amino acid activation	0.000647444
positive regulation of nervous system development	0.000702421
multi-organism behavior	0.000757999
mitochondrial translation	0.000792442
cell development	0.00081763

small GTPase mediated signal transduction	0.000893141
cellular amino acid metabolic process	0.001048413
cellular protein catabolic process	0.001059181
regulation of cellular protein localization	0.001106831
tRNA aminoacylation for protein translation	0.001198
synapse assembly	0.001414982
axon development	0.001449026
vesicle docking	0.001643575
organic acid metabolic process	0.001654424
cytoskeleton organization	0.001769896
establishment of protein localization to organelle	0.001825542
regulation of ion transmembrane transporter activity	0.001847947
regulation of cell development	0.001928895
regulation of catabolic process	0.001981998
protein localization to organelle	0.002020167
cellular component morphogenesis	0.002040554
regulation of dendrite morphogenesis	0.002187294
regulation of protein catabolic process	0.002437635
Ras protein signal transduction	0.002569952
intraspecies interaction between organisms	0.002930703
social behavior	0.002930703
regulation of membrane potential	0.003527003
inorganic cation transmembrane transport	0.003582715
nucleoside phosphate metabolic process	0.004028087
macromolecule catabolic process	0.00413723
nucleotide metabolic process	0.004178744
regulation of transmembrane transporter activity	0.004438101
cell morphogenesis	0.004842568

Enriched protein in co	
Cellular component	
Term	Bonferroni
synapse	2.53391E-40
neuron part	3.97841E-37
synapse part	4.60016E-35
neuron projection	9.10467E-31
membrane-bounded vesicle	6.97978E-27
postsynapse	2.17034E-26
somatodendritic compartment	4.91417E-23
dendrite	8.28198E-22
extracellular exosome	1.23912E-20
extracellular vesicle	1.7826E-20
extracellular organelle	2.89782E-20
excitatory synapse	2.19748E-18
cell junction	6.13952E-18
axon	5.34181E-17
plasma membrane region	6.5395E-17
postsynaptic density	9.54402E-17
postsynaptic specialization	9.54402E-17
synaptic membrane	1.11807E-16
mitochondrion	3.30611E-16
cell body	2.94109E-15
cytosol	1.06704E-14
mitochondrial part	2.04725E-13
postsynaptic membrane	4.0945E-13
neuronal cell body	1.84253E-12
presynapse	5.32285E-12
axon part	3.94096E-11
mitochondrial envelope	2.89072E-10
mitochondrial membrane	4.49781E-10
dendritic spine	1.32519E-09
neuron spine	2.13887E-09
organelle envelope	8.93898E-08
transporter complex	8.95249E-08
mitochondrial inner membrane	1.06604E-07
envelope	1.27158E-07
neuron projection terminus	4.52564E-07
transmembrane transporter complex	1.00727E-06

axon terminus	1.4401E-06
organelle inner membrane	1.12983E-05
ion channel complex	1.16045E-05
endosome	3.52472E-05
adherens junction	0.000139727
cytoplasmic, membrane-bounded vesicle	0.000178242
anchoring junction	0.000253941
cell leading edge	0.000333626
cytoplasmic region	0.000451883
terminal bouton	0.000903436
presynaptic membrane	0.001359724
mitochondrial matrix	0.002408259
endosomal part	0.002503379
cell cortex	0.003355908
vacuole	0.00366096
cell-cell adherens junction	0.004018077
cytoplasmic side of plasma membrane	0.004290597
vacuolar part	0.005152555
early endosome	0.005918605
vacuolar membrane	0.007296669
endosome membrane	0.007777906
dendritic shaft	0.008068578
extracellular region part	0.008933925
exocytic vesicle	0.018876655
cation channel complex	0.019901644
synaptic vesicle	0.019901644
cytoplasmic side of membrane	0.021698577
chaperonin-containing T-complex	0.0234219
oxidoreductase complex	0.03087541
zona pellucida receptor complex	0.032010479
HOPS complex	0.032010479
basolateral plasma membrane	0.038386175
heterotrimeric G-protein complex	0.042823015
AP-type membrane coat adaptor complex	0.045726485

Table 2 GO analysis of common proteins.

common proteins (-1<log_2co/ips<0)	
Biological process	
Term	Bonferroni
cellular amide metabolic process	3.27E-07
peptide metabolic process	3.42E-07
vesicle-mediated transport	1.33E-06
organonitrogen compound biosynthetic process	3.45E-06
translation	5.06E-06
peptide biosynthetic process	1.04E-05
amide biosynthetic process	2.82E-05
regulation of transport	8.75E-05
ribosomal large subunit biogenesis	4.83E-04
cellular component biogenesis	7.31E-04
ribosome biogenesis	0.001439356
protein transport	0.001622627
positive regulation of transport	0.001832954
establishment of protein localization	0.004129276
macromolecule localization	0.006961184
establishment of localization in cell	0.007763547
cellular localization	0.015059269
protein localization	0.015235906
intracellular transport	0.016423039
Golgi vesicle transport	0.017934023
ribonucleoprotein complex biogenesis	0.023187079
response to endoplasmic reticulum stress	0.035236885

common proteins (-1<log$_2$co/ips<0)	
Cellular component	
Term	Bonferroni
ribosomal subunit	1.96E-16
large ribosomal subunit	1.99E-15
ribosome	8.17E-15
cytosolic large ribosomal subunit	1.99E-14
cytosolic ribosome	6.17E-13
adherens junction	4.79E-11
anchoring junction	1.16E-10
membrane-bounded vesicle	1.97E-10
cell junction	1.86E-09
cytosolic part	3.20E-09
extracellular vesicle	7.55E-09
extracellular organelle	8.74E-09
focal adhesion	1.24E-08
extracellular exosome	1.44E-08
cell-substrate adherens junction	1.69E-08
cell-substrate junction	2.27E-08
cytosol	1.09E-07
mitochondrion	4.56E-06
intracellular ribonucleoprotein complex	2.69E-05
ribonucleoprotein complex	2.77E-05
endoplasmic reticulum	6.28E-05
coated vesicle	1.42E-04
cytoplasmic, membrane-bounded vesicle	2.03E-04
melanosome	9.26E-04
pigment granule	9.26E-04
extracellular region part	0.001166484
endoplasmic reticulum part	0.001490788
endosome	0.002982634
vacuole	0.004170797
nuclear outer membrane-endoplasmic reticulum membrane network	0.006112678
cell-cell adherens junction	0.006588786
endoplasmic reticulum membrane	0.009924828
smooth endoplasmic reticulum	0.012228713
mitochondrial part	0.036887442
myelin sheath	0.037679789

common proteins (0<log₂co/ips<1)	
Cellular component	
Term	Bonferroni
membrane-bounded vesicle	3.54279E-45
neuron part	7.66708E-45
neuron projection	4.11618E-40
synapse	3.04852E-39
synapse part	5.57457E-37
extracellular vesicle	6.09763E-36
extracellular organelle	9.44385E-36
extracellular exosome	2.98524E-34
cell junction	1.92449E-31
presynapse	2.40538E-28
myelin sheath	1.0129E-25
axon	2.33081E-25
axon part	1.29177E-22
extracellular region part	5.29529E-16
anchoring junction	5.70718E-16
synaptic vesicle	1.05119E-15
adherens junction	1.59871E-15
terminal bouton	1.80599E-15
exocytic vesicle	3.35952E-15
cell-cell junction	3.44261E-15
cytoplasmic, membrane-bounded vesicle	1.67866E-13
excitatory synapse	1.67866E-13
axon terminus	5.8753E-13
postsynapse	6.71463E-13
transport vesicle	1.84652E-12
cell leading edge	1.93046E-12
dendrite	2.18225E-12
cell-cell adherens junction	2.76978E-12
cytosol	3.18945E-12
somatodendritic compartment	4.36451E-12
neuron projection terminus	5.95923E-12
plasma membrane region	1.45204E-11
extracellular region	7.90648E-11
vacuole	1.05084E-10
postsynaptic specialization	2.38789E-10
postsynaptic density	2.38789E-10

vacuolar membrane	3.36655E-10
vacuolar part	1.95177E-09
synaptic vesicle membrane	2.82669E-09
exocytic vesicle membrane	2.82669E-09
membrane region	4.03474E-09
synaptic membrane	4.39817E-09
secretory vesicle	1.31307E-08
main axon	2.52363E-08
transport vesicle membrane	3.19276E-08
cell body	5.22636E-07
cytoplasmic vesicle part	9.18999E-07
focal adhesion	1.04615E-06
actin cytoskeleton	1.40473E-06
cell-substrate adherens junction	1.5454E-06
melanosome	2.16284E-06
pigment granule	2.16284E-06
cell-substrate junction	2.25924E-06
cytoplasmic vesicle membrane	3.6624E-06
vesicle membrane	6.7099E-06
growth cone	7.73709E-06
cytoplasmic region	1.00491E-05
perinuclear region of cytoplasm	1.00679E-05
site of polarized growth	1.35595E-05
dendritic spine	1.55889E-05
neuron spine	1.99894E-05
leading edge membrane	3.04737E-05
sarcolemma	6.34942E-05
neuronal cell body	6.47291E-05
membrane microdomain	0.000244582
membrane raft	0.000244582
cortical cytoskeleton	0.000366605
cell cortex part	0.000535717
clathrin-coated pit	0.000646763
endosome membrane	0.000764583
mitochondrion	0.000940671
presynaptic membrane	0.000980114
cell projection membrane	0.000994802
lytic vacuole membrane	0.001300423

lysosomal membrane	0.001300423
endosome	0.001464578
endosomal part	0.001829674
SNARE complex	0.002066193
cell-cell contact zone	0.002565178
ruffle	0.002832997
lysosome	0.004074544
lytic vacuole	0.004074544
microtubule	0.004481624
intercalated disc	0.005423005
cell cortex	0.005694108
synaptobrevin 2-SNAP-25-syntaxin-1a complex	0.007717016
paranode region of axon	0.008522101
lamellipodium	0.009155904
supramolecular fiber	0.022990564
polymeric cytoskeletal fiber	0.022990564
microtubule cytoskeleton	0.028175976
postsynaptic membrane	0.036938556
cytoplasmic side of membrane	0.048153731

common proteins (0<log_2co/ips<1)	
Bioogical process	
Term	Bonferroni
vesicle-mediated transport	3.13689E-33
cellular localization	1.71687E-29
regulation of cellular component organization	2.15334E-25
regulation of transport	4.41529E-24
protein localization	1.17211E-23
establishment of protein localization	5.45891E-23
single-organism cellular localization	5.58613E-23
establishment of localization in cell	1.39556E-22
cellular component assembly	1.16953E-21
macromolecule localization	4.79076E-21
cellular component biogenesis	2.27066E-19
cellular protein localization	6.6145E-19
protein transport	7.66582E-19
cellular macromolecule localization	1.2934E-18
membrane organization	6.1211E-18
single-organism membrane organization	7.19303E-18
neuron projection development	9.55512E-18
nervous system development	3.83203E-17
cell projection organization	4.74908E-17
macromolecular complex assembly	6.82003E-17
regulation of cellular component biogenesis	1.0474E-16
regulation of vesicle-mediated transport	1.59392E-16
single-organism organelle organization	1.90828E-16
secretion by cell	3.37106E-16
endomembrane system organization	1.05879E-15
protein complex subunit organization	1.45277E-15
neuron development	1.54286E-15
exocytosis	2.26299E-15
secretion	6.23396E-15
protein complex assembly	6.53938E-15
protein complex biogenesis	6.90502E-15
organelle localization	1.11967E-14
establishment of organelle localization	2.84479E-14
generation of neurons	4.75115E-14
neuron differentiation	5.25741E-14
regulation of neurotransmitter levels	1.13058E-13

trans-synaptic signaling	1.16403E-13
synaptic signaling	1.16403E-13
chemical synaptic transmission	1.16403E-13
anterograde trans-synaptic signaling	1.16403E-13
neurogenesis	1.5066E-13
endocytosis	1.74502E-13
intracellular transport	2.38543E-13
establishment of vesicle localization	6.04961E-13
synaptic vesicle localization	6.04961E-13
vesicle localization	6.04961E-13
regulation of protein complex assembly	6.04961E-13
establishment of synaptic vesicle localization	6.04961E-13
synaptic vesicle transport	6.04961E-13
cytoskeleton organization	1.20992E-12
actin filament-based process	2.41984E-12
neuron projection morphogenesis	2.41984E-12
neurotransmitter transport	3.0248E-12
cellular component morphogenesis	6.04961E-12
synaptic vesicle cycle	6.65457E-12
protein localization to membrane	7.86449E-12
cell morphogenesis	8.46945E-12
regulation of secretion	1.08893E-11
regulation of secretion by cell	1.45191E-11
actin cytoskeleton organization	1.45191E-11
plasma membrane organization	1.93587E-11
intracellular protein transport	2.72232E-11
protein localization to cell periphery	2.96431E-11
vesicle mediated transport in synapse	3.0853E-11
positive regulation of transport	4.29522E-11
regulation of exocytosis	4.96068E-11
signal release from synapse	6.77556E-11
neurotransmitter secretion	6.77556E-11
protein localization to plasma membrane	6.77556E-11
presynaptic process involved in chemical synaptic transmission	1.91772E-10
modulation of synaptic transmission	2.79492E-10
positive regulation of cellular component organization	3.24864E-10
cell part morphogenesis	3.30308E-10
signal release	1.16213E-09

macromolecular complex subunit organization	1.22081E-09
regulated exocytosis	3.82638E-09
cell-cell signaling	5.38717E-09
ion transport	1.04749E-08
cell development	1.30799E-08
cell projection morphogenesis	1.32698E-08
cellular protein complex assembly	1.79328E-08
regulation of cell projection organization	2.03987E-08
calcium ion regulated exocytosis	2.27078E-08
synaptic vesicle exocytosis	3.66352E-08
regulation of organelle organization	4.74483E-08
cellular macromolecular complex assembly	9.11397E-08
actin filament organization	1.55383E-07
regulation of cytoskeleton organization	2.26221E-07
protein polymerization	2.40042E-07
regulation of calcium ion-dependent exocytosis	5.61866E-07
cell morphogenesis involved in neuron differentiation	6.16495E-07
regulation of cellular localization	1.62966E-06
regulation of neuron differentiation	1.68844E-06
cell morphogenesis involved in differentiation	1.72833E-06
regulation of protein polymerization	3.46995E-06
establishment of protein localization to membrane	6.81516E-06
lamellipodium organization	6.83412E-06
regulation of neuron projection development	7.52114E-06
cation transport	1.27274E-05
establishment of protein localization to plasma membrane	1.33959E-05
regulation of cell morphogenesis	1.35775E-05
regulation of actin filament-based process	1.87319E-05
regulation of nervous system development	2.11679E-05
negative regulation of cellular component organization	2.8491E-05
regulation of neurogenesis	3.20115E-05
regulation of protein localization	3.46784E-05
regulation of endocytosis	3.60125E-05
receptor-mediated endocytosis	3.7304E-05
microtubule-based process	4.12748E-05
regulation of cell development	4.36757E-05
actin filament polymerization	6.05884E-05
axon development	6.82265E-05

transmembrane transport	8.63125E-05
metal ion transport	0.000100556
regulation of synaptic plasticity	0.000114747
single-organism intracellular transport	0.000138294
actin polymerization or depolymerization	0.000173407
regulation of cellular component size	0.000174378
regulation of actin cytoskeleton organization	0.00020695
negative regulation of protein complex assembly	0.00021169
cellular protein complex disassembly	0.00021169
axonogenesis	0.000267333
lamellipodium assembly	0.000273261
regulation of actin filament polymerization	0.000278826
positive regulation of cellular component biogenesis	0.000318233
regulation of ion transport	0.000327794
vacuolar transport	0.000364464
ion transmembrane transport	0.000367342
regulation of regulated secretory pathway	0.000372674
membrane fusion	0.000442098
regulation of actin polymerization or depolymerization	0.000489559
regulation of actin filament length	0.000541675
monovalent inorganic cation transport	0.000865495
regulation of establishment of protein localization	0.000914535
synaptic vesicle recycling	0.001142657
regulation of synapse structure or activity	0.00122179
regulation of anatomical structure size	0.001888889
regulation of metal ion transport	0.002239368
dendrite development	0.002734764
protein oligomerization	0.002822178
vesicle organization	0.003206627
cell junction assembly	0.003385074
biological adhesion	0.003523873
regulation of hormone levels	0.003644148
central nervous system development	0.003674785
movement of cell or subcellular component	0.003784436
brain development	0.003964506
protein homooligomerization	0.004471542
cell adhesion	0.004931025
regulation of anatomical structure morphogenesis	0.00658615

Golgi vesicle transport	0.00684439
protein complex disassembly	0.007630522
regulation of membrane potential	0.008333813
organelle fusion	0.008391334
cellular component disassembly	0.008565703
regulation of ion transmembrane transport	0.008800217
nitrogen compound transport	0.00884804
regulation of protein localization to plasma membrane	0.011458687
positive regulation of cell projection organization	0.011534594
cellular homeostasis	0.011568308
regulation of protein localization to cell periphery	0.013316819
hormone transport	0.014381305
positive regulation of organelle organization	0.015318926
regulation of protein transport	0.016844385
positive regulation of cytoskeleton organization	0.01890281
macromolecular complex disassembly	0.020702419
head development	0.021165536
regulation of transmembrane transport	0.021384181
glutamate receptor signaling pathway	0.022182122
endosomal transport	0.023393484
cell junction organization	0.023794825
hormone secretion	0.026869729
locomotion	0.028765176
protein targeting	0.031900998
positive regulation of protein complex assembly	0.032129823
positive regulation of nervous system development	0.034037188
actin filament bundle assembly	0.034816061
actin filament bundle organization	0.045713913
regulation of plasma membrane organization	0.045730934

Chapter 5. References

BANDRES-CIGA, S., SAEZ-ATIENZAR, S., BONET-PONCE, L., BILLINGSLEY, K., VITALE, D., BLAUWENDRAAT, C., GIBBS, J. R., PIHLSTRøM, L., GAN-OR, Z., CONSORTIUM, T. I. P. S. D. G., COOKSON, M. R., NALLS, M. A. & SINGLETON, A. B. 2019. The endocytic membrane trafficking pathway plays a major role in the risk of Parkinson's disease. *Movement Disorders,* 34**,** 460-468.

BRAAK, H. & DEL TREDICI, K. 2017. Neuropathological Staging of Brain Pathology in Sporadic Parkinson's disease: Separating the Wheat from the Chaff. *J Parkinsons Dis,* 7**,** S71-S85.

BRAAK, H., TREDICI, K. D., RUB, U., DE VOS, R. A. I., JANSEN STEUR, E. N. H. & BRAAK, E. 2003. Staging of brain pathology related to sporadic Parkinson's disease. *Neurobiology of Aging,* 24**,** 197-211.

BRAHIC, M., BOUSSET, L., BIERI, G., MELKI, R. & GITLER, A. D. 2016. Axonal transport and secretion of fibrillar forms of alpha-synuclein, Abeta42 peptide and HTTExon 1. *Acta Neuropathol,* 131**,** 539-48.

BRIDI, J. C. & HIRTH, F. 2018. Mechanisms of alpha-Synuclein Induced Synaptopathy in Parkinson's Disease. *Front Neurosci,* 12**,** 80.

BURRé, J., SHARMA, M. & SUDHOF, T. C. 2014. α-Synuclein assembles into higher-order multimers upon membrane binding to promote SNARE complex formation. *Proceedings of the National Academy of Sciences,* 111**,** E4274-E4283.

CHIVET, M., JAVALET, C., LAULAGNIER, K., BLOT, B., HEMMING, F. J. & SADOUL, R. 2014. Exosomes secreted by cortical neurons upon glutamatergic synapse activation specifically interact with neurons. *J Extracell Vesicles,* 3**,** 24722.

COOPER, A. A., GITLER, A. D., CASHIKAR, A., HAYNES, C. M., HILL, K. J., BHULLAR, B., LIU, K., XU, K., STRATHEARN, K. E., LIU, F., CAO, S., CALDWELL, K. A., CALDWELL, G. A., MARSISCHKY, G., KOLODNER, R. D., LABAER, J., ROCHET, J.-C., BONINI, N. M. & LINDQUIST, S. 2006. α-Synuclein Blocks ER-Golgi Traffic and Rab1 Rescues Neuron Loss in Parkinson's Models. *Science,* 313**,** 324.

DI MAIO, R., BARRETT, P. J., HOFFMAN, E. K., BARRETT, C. W., ZHARIKOV, A., BORAH, A., HU, X., MCCOY, J., CHU, C. T., BURTON, E. A., HASTINGS, T. G. & GREENAMYRE, J. T. 2016. α-Synuclein binds to TOM20 and inhibits mitochondrial protein import in Parkinson's disease. *Science Translational Medicine,* 8**,** 342ra78-342ra78.

EMAMZADEH, F. N. 2016. Alpha-synuclein structure, functions, and interactions. *Journal of research in medical sciences : the official journal of Isfahan University of Medical Sciences,* 21**,** 29-29.

FROULA, J. M., HENDERSON, B. W., GONZALEZ, J. C., VADEN, J. H., MCLEAN, J. W., WU, Y., BANUMURTHY, G., OVERSTREET-WADICHE, L., HERSKOWITZ, J. H. & VOLPICELLI-DALEY, L. A. 2018. alpha-Synuclein fibril-induced paradoxical structural and functional defects in hippocampal neurons. *Acta Neuropathol Commun,* 6**,** 35.

GEORGE, S. & BRUNDIN, P. 2015. Immunotherapy in Parkinson's Disease: Micromanaging Alpha-Synuclein Aggregation. *J Parkinsons Dis,* 5**,** 413-24.

GEORGE, S., REY, N. L., TYSON, T., ESQUIBEL, C., MEYERDIRK, L., SCHULZ, E., PIERCE, S., BURMEISTER, A. R., MADAJ, Z., STEINER, J. A., ESCOBAR GALVIS, M. L., BRUNDIN, L. & BRUNDIN, P. 2019. Microglia affect α-synuclein cell-to-cell transfer in a mouse model of Parkinson's disease. *Molecular Neurodegeneration,* 14.

GIAIME, E., TONG, Y., WAGNER, L. K., YUAN, Y., HUANG, G. & SHEN, J. 2017. Age-Dependent Dopaminergic Neurodegeneration and Impairment of the Autophagy-Lysosomal Pathway in LRRK-Deficient Mice. *Neuron,* 96**,** 796-807 e6.

GOEDERT, M. 2015. NEURODEGENERATION. Alzheimer's and Parkinson's diseases: The prion concept in relation to assembled Abeta, tau, and alpha-synuclein. *Science,* 349**,** 1255555.

GONDA, A., KABAGWIRA, J., SENTHIL, G. N. & WALL, N. R. 2019. Internalization of Exosomes through Receptor-Mediated Endocytosis. *Mol Cancer Res,* 17**,** 337-347.

GRIBAUDO, S., TIXADOR, P., BOUSSET, L., FENYI, A., LINO, P., MELKI, R., PEYRIN, J. M. & PERRIER, A. L. 2019. Propagation of alpha-Synuclein Strains within Human Reconstructed Neuronal Network. *Stem Cell Reports,* 12**,** 230-244.

GUO, M., WANG, J., ZHAO, Y., FENG, Y., HAN, S., DONG, Q., CUI, M. & TIEU, K. 2020. Microglial exosomes facilitate alpha-synuclein transmission in Parkinson's disease. *Brain,* 143**,** 1476-1497.

GYLYS, K. H. & BILOUSOVA, T. 2017. Flow Cytometry Analysis and Quantitative Characterization of Tau in Synaptosomes from Alzheimer's Disease Brains. *Methods Mol Biol,* 1523**,** 273-284.

HAYES, M. T. 2019. Parkinson's Disease and Parkinsonism. *Am J Med,* 132**,** 802-807.

HENDERSON, M. X., CORNBLATH, E. J., DARWICH, A., ZHANG, B., BROWN, H., GATHAGAN, R. J., SANDLER, R. M., BASSETT, D. S., TROJANOWSKI, J. Q. & LEE, V. M. Y. 2019. Spread of alpha-synuclein pathology through the brain connectome is modulated by selective vulnerability and predicted by network analysis. *Nat Neurosci,* 22**,** 1248-1257.

HERNANDEZ, S. M., TIKHONOVA, E. B. & KARAMYSHEV, A. L. 2020. Protein-Protein Interactions in Alpha-Synuclein Biogenesis: New Potential Targets in Parkinson's Disease. *Frontiers in Aging Neuroscience,* 12.

HIROKAWA, N., NIWA, S. & TANAKA, Y. 2010. Molecular motors in neurons: transport mechanisms and roles in brain function, development, and disease. *Neuron,* 68**,** 610-38.

HOLMES, B. B., DEVOS, S. L., KFOURY, N., LI, M., JACKS, R., YANAMANDRA, K., OUIDJA, M. O., BRODSKY, F. M., MARASA, J., BAGCHI, D. P., KOTZBAUER, P. T., MILLER, T. M., PAPY-GARCIA, D. & DIAMOND, M. I. 2013. Heparan sulfate proteoglycans mediate internalization and propagation of specific proteopathic seeds. *Proc Natl Acad Sci U S A,* 110**,** E3138-47.

HSU, L. J., SAGARA, Y., ARROYO, A., ROCKENSTEIN, E., SISK, A., MALLORY, M., WONG, J., TAKENOUCHI, T., HASHIMOTO, M. & MASLIAH, E. 2000. α -Synuclein Promotes Mitochondrial Deficit and Oxidative Stress. *The American Journal of Pathology,* 157**,** 401-410.

HUANG DA, W., SHERMAN, B. T. & LEMPICKI, R. A. 2009. Systematic and integrative analysis of large gene lists using DAVID bioinformatics resources. *Nat Protoc,* 4**,** 44-57.

IRWIN, D. J., WHITE, M. T., TOLEDO, J. B., XIE, S. X., ROBINSON, J. L., VAN DEERLIN, V., LEE, V. M.-Y., LEVERENZ, J. B., MONTINE, T. J., DUDA, J. E., HURTIG, H. I. & TROJANOWSKI, J. Q. 2012. Neuropathologic substrates of Parkinson disease dementia. *Annals of Neurology,* 72**,** 587-598.

JASSAL, B., MATTHEWS, L., VITERI, G., GONG, C., LORENTE, P., FABREGAT, A., SIDIROPOULOS, K., COOK, J., GILLESPIE, M., HAW, R., LONEY, F., MAY, B., MILACIC, M., ROTHFELS, K., SEVILLA, C., SHAMOVSKY, V., SHORSER, S., VARUSAI, T., WEISER, J., WU, G., STEIN, L., HERMJAKOB, H. & D'EUSTACHIO, P. 2020. The reactome pathway knowledgebase. *Nucleic acids research,* 48**,** D498-D503.

KAHLE, P. J., NEUMANN, M., OZMEN, L., MULLER, V., JACOBSEN, H., SCHINDZIELORZ, A., OKOCHI, M., LEIMER, U., VAN DER PUTTEN, H., PROBST, A., KREMMER, E., KRETZSCHMAR, H. A. & HAASS, C. 2000. Subcellular localization of wild-type and Parkinson's disease-associated mutant alpha -synuclein in human and transgenic mouse brain. *J Neurosci,* 20**,** 6365-73.

KAWAI, S., TAKAGI, Y., KANEKO, S. & KUROSAWA, T. 2011. Effect of Three Types of Mixed Anesthetic Agents Alternate to Ketamine in Mice. *Experimental Animals,* 60**,** 481-487.

KORDOWER, J. H., CHU, Y., HAUSER, R. A., FREEMAN, T. B. & OLANOW, C. W. 2008. Lewy body-like pathology in long-term embryonic nigral transplants in Parkinson's disease. *Nat Med,* 14**,** 504-6.

LEE, H. J., SUK, J. E., BAE, E. J., LEE, J. H., PAIK, S. R. & LEE, S. J. 2008. Assembly-dependent endocytosis and clearance of extracellular alpha-synuclein. *Int J Biochem Cell Biol,* 40**,** 1835-49.

LI, J. Y., ENGLUND, E., HOLTON, J. L., SOULET, D., HAGELL, P., LEES, A. J., LASHLEY,

T., QUINN, N. P., REHNCRONA, S., BJORKLUND, A., WIDNER, H., REVESZ, T., LINDVALL, O. & BRUNDIN, P. 2008. Lewy bodies in grafted neurons in subjects with Parkinson's disease suggest host-to-graft disease propagation. *Nat Med,* 14, 501-3.

LUK, K. C., KEHM, V., CARROLL, J., ZHANG, B., O'BRIEN, P., TROJANOWSKI, J. Q. & LEE, V. M. 2012. Pathological α-synuclein transmission initiates Parkinson-like neurodegeneration in nontransgenic mice. *Science,* 338, 949-53.

MAO, X., OU, M. T., KARUPPAGOUNDER, S. S., KAM, T. I., YIN, X., XIONG, Y., GE, P., UMANAH, G. E., BRAHMACHARI, S., SHIN, J. H., KANG, H. C., ZHANG, J., XU, J., CHEN, R., PARK, H., ANDRABI, S. A., KANG, S. U., GONCALVES, R. A., LIANG, Y., ZHANG, S., QI, C., LAM, S., KEILER, J. A., TYSON, J., KIM, D., PANICKER, N., YUN, S. P., WORKMAN, C. J., VIGNALI, D. A., DAWSON, V. L., KO, H. S. & DAWSON, T. M. 2016. Pathological alpha-synuclein transmission initiated by binding lymphocyte-activation gene 3. *Science,* 353.

MASUDA-SUZUKAKE, M., NONAKA, T., HOSOKAWA, M., KUBO, M., SHIMOZAWA, A., AKIYAMA, H. & HASEGAWA, M. 2014. Pathological alpha-synuclein propagates through neural networks. *Acta Neuropathol Commun,* 2, 88.

MUñOZ, E., OLIVA, R., OBACH, V., MARTı´, M. A. J., PASTOR, P., BALLESTA, F. & TOLOSA, E. 1997. Identification of Spanish familial Parkinson's disease and screening for the Ala53Thr mutation of the α-synuclein gene in early onset patients. *Neuroscience Letters,* 235, 57-60.

NGOLAB, J., TRINH, I., ROCKENSTEIN, E., MANTE, M., FLORIO, J., TREJO, M., MASLIAH, D., ADAME, A., MASLIAH, E. & RISSMAN, R. A. 2017. Brain-derived exosomes from dementia with Lewy bodies propagate alpha-synuclein pathology. *Acta Neuropathol Commun,* 5, 46.

OKUZUMI, A., KUROSAWA, M., HATANO, T., TAKANASHI, M., NOJIRI, S., FUKUHARA, T., YAMANAKA, T., MIYAZAKI, H., YOSHINAGA, S., FURUKAWA, Y., SHIMOGORI, T., HATTORI, N. & NUKINA, N. 2018. Rapid dissemination of alpha-synuclein seeds through neural circuits in an in-vivo prion-like seeding experiment. *Acta Neuropathol Commun,* 6, 96.

POLYMEROPOULOS, M. H., LAVEDAN, C., LEROY, E., IDE, S. E., DEHEJIA, A., DUTRA, A., PIKE, B., ROOT, H., RUBENSTEIN, J., BOYER, R., STENROOS, E. S., CHANDRASEKHARAPPA, S., ATHANASSIADOU, A., PAPAPETROPOULOS, T., JOHNSON, W. G., LAZZARINI, A. M., DUVOISIN, R. C., DI IORIO, G., GOLBE, L. I. & NUSSBAUM, R. L. 1997. Mutation in the α-Synuclein Gene Identified in Families with Parkinson's Disease. *Science,* 276, 2045.

RUSSO, I., BUBACCO, L. & GREGGIO, E. 2012. Exosomes-associated neurodegeneration and

progression of Parkinson's disease. *American journal of neurodegenerative disease,* 1, 217-225.

SATORI, C. P., KOSTAL, V. & ARRIAGA, E. A. 2012. Review on recent advances in the analysis of isolated organelles. *Anal Chim Acta,* 753, 8-18.

SHALIT, T., ELINGER, D., SAVIDOR, A., GABASHVILI, A. & LEVIN, Y. 2015. MS1-Based Label-Free Proteomics Using a Quadrupole Orbitrap Mass Spectrometer. *Journal of Proteome Research,* 14, 1979-1986.

SINGLETON, A. B., FARRER, M., JOHNSON, J., SINGLETON, A., HAGUE, S., KACHERGUS, J., HULIHAN, M., PEURALINNA, T., DUTRA, A., NUSSBAUM, R., LINCOLN, S., CRAWLEY, A., HANSON, M., MARAGANORE, D., ADLER, C., COOKSON, M. R., MUENTER, M., BAPTISTA, M., MILLER, D., BLANCATO, J., HARDY, J. & GWINN-HARDY, K. 2003. alpha-Synuclein locus triplication causes Parkinson's disease. *Science,* 302, 841.

SOTO, C. 2001. Protein misfolding and disease; protein refolding and therapy. *FEBS Letters,* 498, 204-207.

SPILLANTINI, M. G., SCHMIDT, M. L., LEE, V. M. Y., TROJANOWSKI, J. Q., JAKES, R. & GOEDERT, M. 1997. α-Synuclein in Lewy bodies. *Nature,* 388, 839-840.

TANEI, T., PRADIPTA, A. R., MORIMOTO, K., FUJII, M., ARATA, M., ITO, A., YOSHIDA, M., SAIGITBATALOVA, E., KURBANGALIEVA, A., IKEDA, J. I., MORII, E., NOGUCHI, S. & TANAKA, K. 2019. Cascade Reaction in Human Live Tissue Allows Clinically Applicable Diagnosis of Breast Cancer Morphology. *Adv Sci (Weinh),* 6, 1801479.

TYSNES, O. B. & STORSTEIN, A. 2017. Epidemiology of Parkinson's disease. *J Neural Transm (Vienna),* 124, 901-905.

VOLPICELLI-DALEY, L. A., LUK, K. C., PATEL, T. P., TANIK, S. A., RIDDLE, D. M., STIEBER, A., MEANEY, D. F., TROJANOWSKI, J. Q. & LEE, V. M. 2011. Exogenous α-synuclein fibrils induce Lewy body pathology leading to synaptic dysfunction and neuron death. *Neuron,* 72, 57-71.

VON BARTHELD, C. S. & ALTICK, A. L. 2011. Multivesicular bodies in neurons: Distribution, protein content, and trafficking functions. *Progress in Neurobiology,* 93, 313-340.

WANG, H., IMAMURA, Y., ISHIBASHI, R., CHANDANA, E. P., YAMAMOTO, M. & NODA, M. 2010. The Reck tumor suppressor protein alleviates tissue damage and promotes functional recovery after transient cerebral ischemia in mice. *J Neurochem,* 115, 385-98.

WIŚNIEWSKI, J. R., ZOUGMAN, A., NAGARAJ, N. & MANN, M. 2009. Universal sample preparation method for proteome analysis. *Nat Methods,* 6, 359-62.

WONG, Y. C. & KRAINC, D. 2017. alpha-synuclein toxicity in neurodegeneration: mechanism

and therapeutic strategies. *Nat Med,* 23, 1-13.

YONEKAWA, Y., HARADA, A., OKADA, Y., FUNAKOSHI, T., KANAI, Y., TAKEI, Y., TERADA, S., NODA, T. & HIROKAWA, N. 1998. Defect in synaptic vesicle precursor transport and neuronal cell death in KIF1A motor protein-deficient mice. *The Journal of cell biology,* 141, 431-441.